conjugated anti-CD31 antibody (1:300; BD Pharmingen). Stained cells were photographed with inverted fluorescent microscopy, Eclipse TE2000-U (Nikon) and digital camera system AxioCam HRc with the use of AxioVision Software (Carl Zeiss), or confocal fluorescent microscopy (TCS SP2; Leica).

Immunostaining for three-dimensional culture

Immunostaining for vascular structures in type I collagen gel was performed after the whole-mount immunostaining procedure as described.[25] In brief, gels were fixed with 4% paraformaldehyde and blocked by 1% skim milk/0.1% Triton X/phosphate-buffered saline solution and incubated with anti-CD31 (BD Pharmingen) and anti–α smooth muscle actin (αSMA; Sigma-Aldrich), or anti-NRP1 (R&D Systems) and anti-Flk1 antibodies (1:200). Alexa Fluor 488–conjugated anti–mouse or anti–goat IgG and Alexa Fluor 567–conjugated anti–rat IgG (1:500; Zymed) were used as secondary antibodies. Alternatively, anti–rat IgG conjugated with alkaline phosphatase and anti–mouse IgG conjugated with horseradish peroxidase (Zymed) were used as secondary antibodies for enzymatic color development.

Cross-section of three-dimensional culture and immunostaining

Gel clots including vascular structure were fixed in 3.7% formaldehyde for 24 hours. Paraffin-embedded gel clots were sectioned at 3-μm thickness. The sections were mounted on glass slides coated with 2% 3-aminopropyl triethoxy silane (Tokyo Kasei). After deparaffinization and washing in distilled water, hematoxylin-eosin or immunohistochemical staining was performed.[30] For double immunostaining for CD31 and SMA, CD31 was first stained with whole-mount in-gel staining using anti-CD31 antibody and anti–rat IgG antibody conjugated with horseradish peroxidase. Subsequently, gel clots were subjected to paraffin embedding. Anti-SMA antibody (1:100; DAKO) was applied to sectioned slides overnight at 4°C. They were incubated with biotinylated horse anti–mouse serum diluted to 1:300 followed by streptavidin-alkaline phosphatase.

RNA isolation, RT-PCR, and quantitative RT-PCR

Total RNA was isolated from cells in Dox treatment or Dox-free condition at Flk-d3 using RNeasy (QIAGEN), according to the manufacturer's instructions. Reverse-transcription was performed with the SuperScript III first-strand synthesis system (Invitrogen). Reverse-transcription (RT)–PCR was carried out as described[26] using indicated primers (supplemental Table 1). Quantitative RT-PCR was performed using Power SYBR Green PCR Master Mix (Applied Biosystems) and StepOnePlus system (Applied Biosystems). The amount of target RNA was determined from the appropriate standard curve and normalized relative to the amount of *Gapdh* mRNA. Primer sequences are shown in supplemental Table 2.

Immunoprecipitation and immunoblotting

Immunoprecipitation and immunoblotting were performed according to the report by Pan et al.[31] In brief, $Flk1^+$ cells were incubated with vehicle, anti-VEGF (5 μg/mL), or anti-NRP1 antibodies (5 μg/mL; R&D Systems) in serum-free medium, SFO3 (Sanko Junyaku),[25] for 30 minutes at 37°C. Cells were then cooled on ice for 15 minutes, and VEGF isoforms were added, followed by 30-minute incubation at 4°C. Cells were stimulated for 7 minutes at 37°C and then washed with ice-cold phosphate-buffered saline and lysed in lysis buffer. Cell lysates were subjected to immunoprecipitation using Protein G HP SpinTrap (GE Healthcare) and anti-Flk1 antibody, and immunoblotted with antibodies specific for NRP1 (R&D Systems). Samples were run on sodium dodecyl sulfate/polyacrylamide gel electrophoresis using gradient gel (Atto Co) followed by electrophoretic transfer onto nitrocellulose membranes. After the blots were incubated for 1 hour in blocking agents Blocking One (Nacalai Tesque), they were incubated overnight with the respective NRP1 antibodies (0.5 μg/mL; R&D Systems). Horseradish peroxidase–conjugated anti–goat antibody (Zymed Laboratories) was used as secondary antibody (1:1000). Can Get Signal Immunoreaction Enhancer solution kit (Toyobo) was used for signal enhancement. Immunoreactivity was detected with the enhanced chemiluminescence kit Chemi-Lumi One (Nacalai Tesque).

Ex vivo whole-embryo culture

Embryos were dissected out of the deciduum and placed in 500 μL dimethyl ether containing 50% rat IC serum (Charles River Laboratories), 5 mM nonessential amino acids, 50 mM sodium pyruvate, and 27.5 mM 2-mercaptoethanol, pre-equilibrated at 37°C with 5% CO_2. Embryos were cultured at 37°C with 5% CO_2 and analyzed. H89 (dissolved in dimethyl sulfoxide) was used at 30 μM. The concentration of dimethyl sulfoxide was set at 0.3% in all cultures.[32] Whole-mount staining of embryos and yolk sacs was performed as described previously,[33] and microscopy was performed using a microscope (MZ6; Leica) with 5× objectives (Leica 10411589). Images were imported using Adobe Photoshop software, and quantification of whole yolk sacs and CD31-stained areas was performed using ImageJ software (National Institutes of Health). Results of quantification were expressed as ratio of $CD31^+$/whole yolk sac area, which provides an estimate of the proportion of the yolk sacs that were occupied by CD31-stained vascular structures. Animal experiments were done under the approval of the Animal Research Committee of Kyoto University in accordance with the guidelines for animal experiments in the Guide for the Care and Use of Laboratory Animals in Japan.

Statistical analysis

At least 3 independent experiments were performed. Statistical analysis of the data was performed with the Student *t* test or analysis of variance. *P* values less than .05 was considered significant. Values are reported as means plus or minus SD.

Results

cAMP/PKA pathway plays a critical role in vascular development

In our ES cell differentiation system, first we induced $Flk1^+$ progenitor cells from undifferentiated ES cells. $Flk1^+$ cells that appeared after 96 to 108 hours of differentiation of undifferentiated ES cells were negative for EC markers, such as CD31 and VE-cadherin.[24-26] Then, purified $Flk1^+$ progenitor cells were cultured for further differentiation to vascular cells. As previously reported, whereas no $CD31^+$ ECs appeared when $Flk1^+$ cells were cultured for 3 days with DM ("Methods") alone, addition of VEGF to the $Flk1^+$ cell culture induced selective appearance of $CD31^+$ ECs and SMA^+ MCs (Figure 1A).[25,26] Almost all of $CD31^+$ cells were also positive for other EC markers, VE-cadherin, claudin-5, and eNOS (Figure 1A-B).[25,26] SMA^+ MCs, which were reciprocally negative for EC markers (Figure 1B), expressed other smooth muscle cell markers, SM22α and calponin (Figure 1A). In this culture condition, only these 2 cell types (ie, ECs and MCs), and no blood cells such as $CD45^+$ cells, were specifically induced from $Flk1^+$ cells (Figure 1C).[26]

Stimulation of cAMP signaling by addition of 8bromo-cAMP, an analog of cAMP, together with VEGF substantially enhanced $CD31^+$ EC induction from $Flk1^+$ cells (Figure 2A-B). Similar to ECs induced by VEGF alone (Figure 1), $CD31^+$ ECs that appeared by treatment of 8bromo-cAMP and VEGF were also positive for other EC markers, VE-cadherin, eNOS, and claudin5, but not CD45 (supplemental Figure 2). Compared with VEGF alone, VEGF with 8bromo-cAMP induced approximately 2-fold increase in EC population ($CD31^+$ cells: 26.5% ± 2.3% in VEGF alone vs 52.3% ± 2.7% in VEGF with 8bromo-cAMP, n = 16; $P < .001$; Figure 2C). Total EC numbers induced from the same number of $Flk1^+$ cells were similarly increased approximately 2.3 times by 8bromo-cAMP treatment ($CD31^+$ cells: 9.4 ± 0.8 [× 10^4] cells in VEGF alone vs 21.8 ± 0.9 [× 10^4] cells in VEGF with 8bromo-cAMP; n = 4; $P < .001$; Figure 2D). PKA inhibitors, PKI and

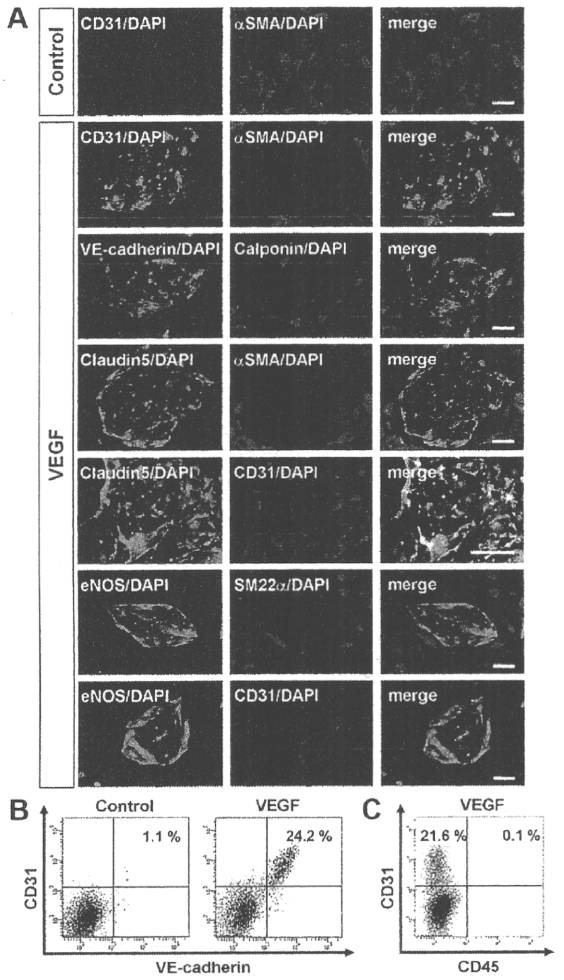

Figure 1. Vascular endothelial growth factor induces endothelial cells from vascular progenitors. (A-C) Cells after three-dimensional culture of Flk1$^+$ cells (Flk-d3). (A-B) Exclusive induction of endothelial cells (ECs) and mural cells (MCs) from Flk1$^+$ cells. (A) Expression of EC and MC markers. (Top panels) Double immunostaining of CD31 (green) and αSMA (red) cultured with differentiation medium (DM) alone (control). Note that no CD31$^+$ cells appeared. (Other panels) Vascular endothelial growth factor (VEGF) treatment (50 ng/mL). EC sheets appeared. Double staining with pan-EC markers (CD31, VE-cadherin, Claudin5, or eNOS; green) and MC markers (αSMA, SM22α, or Calponin; red). (Bottom panels) Double staining with eNOS (green) and CD31 (red). ECs and MCs were exclusively induced. Nuclei are stained with DAPI (blue). Scale bar represents 50 μm. (B) Flow cytometry. x-axis: VE-cadherin; y-axis: CD31. Percentages of CD31$^+$/VE-cadherin$^+$ ECs in total Flk1$^+$ cell–derived cells are indicated. (C) Flow cytometry. x-axis: CD45; y-axis: CD31. Percentages of CD31$^+$/CD45$^-$ ECs and CD31$^+$/CD45$^+$ blood cells in total Flk1$^+$ cell–derived cells are indicated. Note that almost no CD45$^+$ cells were induced in this culture.

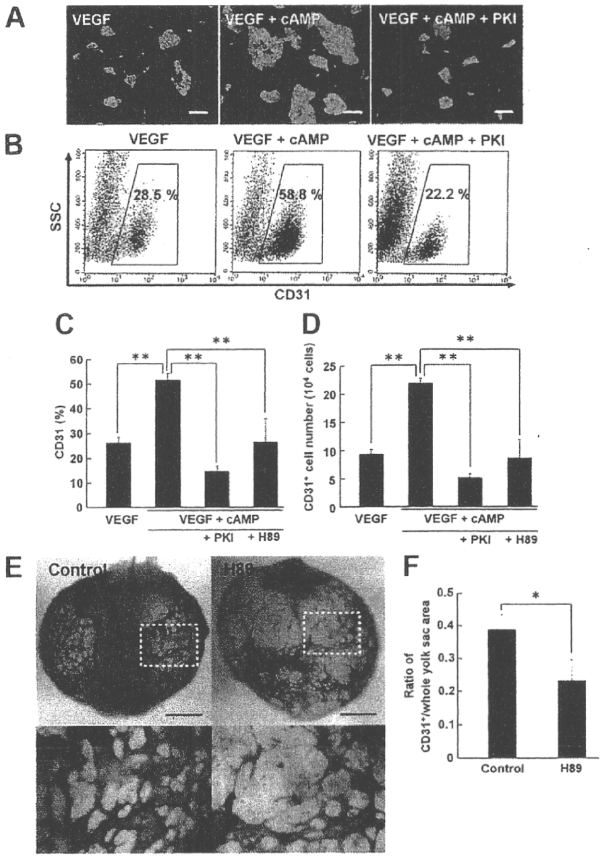

Figure 2. Cyclic adenosine monophosphate/protein kinase A pathway plays a critical role in vascular development. (A-D) Enhancement of EC induction by cyclic adenosine monophosphate (cAMP) through protein kinase A (PKA) at Flk-d3. (A) Fluorescent staining for CD31 (green). (Left panel) VEGF treatment alone (50 ng/mL). (Middle panel) VEGF with 8bromo-cAMP (0.5 mM). (Right panel) VEGF with 8bromo-cAMP and PKA inhibitor, PKI (10 μM). Nuclei are stained with DAPI (blue). Scale bars represent 250 μm. (B) Flow cytometry. x-axis: CD31; y-axis: side scatter (SSC). Percentages of CD31$^+$ ECs in total Flk1$^+$ cell–derived cells are indicated. (C-D) Quantitative evaluation of the effect of PKA inhibitors on CD31$^+$ EC induction from Flk1$^+$ cells by FACS. (C) Percentages of CD31$^+$ cell population in total Flk1$^+$ cell–derived cells. VEGF (50 ng/mL; n = 16); VEGF and 8bromo-cAMP (0.5 mM; n = 16); VEGF, cAMP, and PKI (10 μM; n = 7); and VEGF, cAMP, and H89 (10 μM; n = 6) treatment are shown (**$P < .01$ vs VEGF and 8bromo-cAMP). (D) CD31$^+$ cell number that appeared from 1.5 × 10^5 Flk1$^+$ cells. VEGF (50 ng/mL; n = 4); VEGF and 8bromo-cAMP (0.5 mM; n = 4); VEGF, cAMP, and PKI (10 μM; n = 4); and VEGF, cAMP, and H89 (10 μM; n = 4) treatment are shown (**$P < .01$ vs VEGF and 8bromo-cAMP). (E-F) Role of PKA in vascular formation in the embryo. (E) Representative results of ex vivo culture of mouse embryo. Isolated E6.75 concepti were cultured in the absence (control, left panels) or presence (right panels) of H89 (30 μM) for 3 days. Vasculature in yolk sacs of concepti was immunostained for CD31 (purple). Bottom panels correspond to boxed regions in control and H89, respectively. Apparent reduction of CD31$^+$ vascular formation was induced by H89 treatment. Scale bar represents 1 mm. (F) Quantitative evaluation of CD31$^+$ vasculature formation in yolk sacs of concepti. The ratio of CD31$^+$/whole yolk sac area was evaluated (n = 3; *$P < .05$ vs control).

H89, but not many other kinase inhibitors ("Methods"), specifically inhibited the cAMP effects on EC induction (Figure 2A-D). These results indicated that the cAMP/PKA pathway specifically enhances the effect of VEGF on EC differentiation from Flk1$^+$ progenitor cells.

We further examined the role of PKA in vascular development with ex vivo whole-embryo culture assay. Embryonic day 6.75 concepti were picked out from the uteri of pregnant mice and cultured for 3 days, during which CD31$^+$ blood vessels were formed in the yolk sac. Using this system, we could examine early phase of EC differentiation ex vivo. In the presence of H89 during ex vivo culture, formation of blood vessels, which were evaluated by CD31 staining, in yolk sac was markedly disturbed, showing malformation of vascular networks with decrease in the caliber size and CD31$^+$ areas (Figure 2E). Indeed, CD31$^+$ area within whole yolk sac area was significantly decreased in H89-treated embryo to approximately 59% of that in control (n = 3; $P = .025$; Figure 2F). These results indicate that PKA also plays an important role in early vascular development in vivo.

CA-PKA enhanced EC differentiation and vascular formation from Flk1$^+$ vascular progenitors

To dissect PKA function in EC differentiation, we generated ES cells expressing CA-PKA by tetracycline-regulatable system (Tet-Off; supplemental Figure 1). Although negative effects of high-dose Dox (~ 25 μg/mL) on EC differentiation, proliferation, and survival were

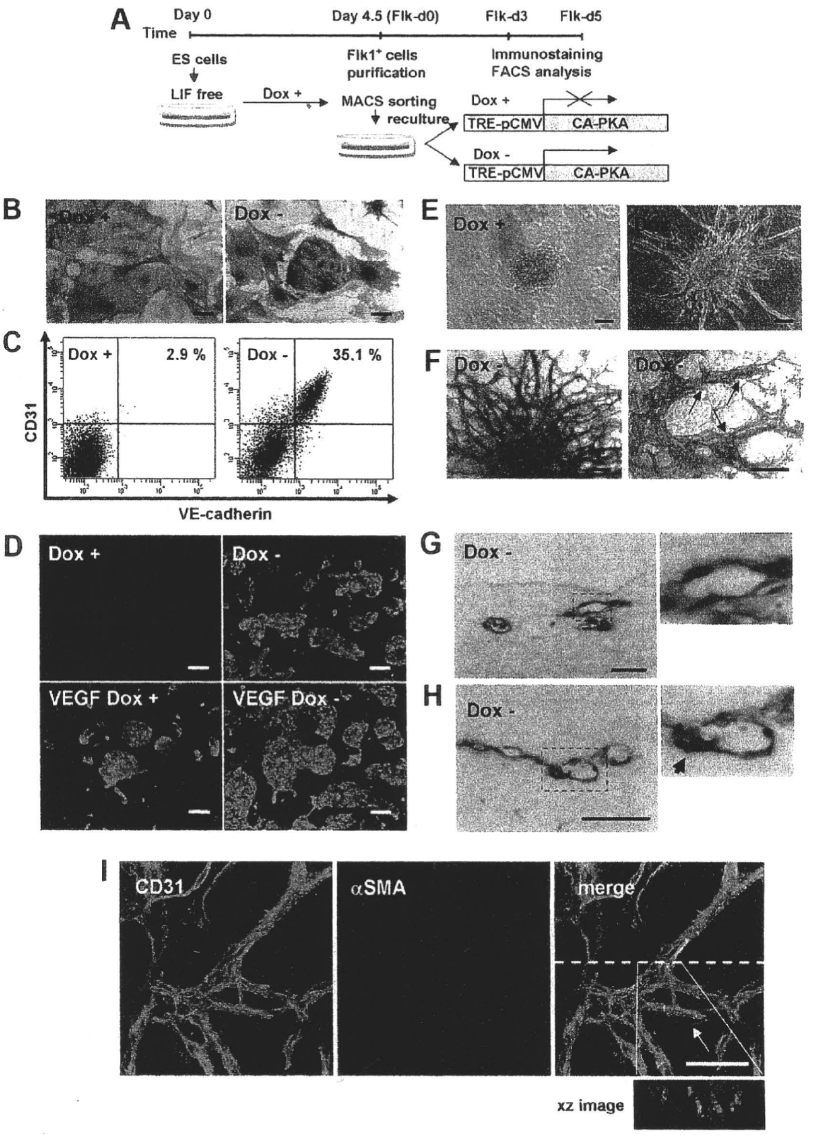

Figure 3. CA-PKA enhances EC differentiation from Flk1$^+$ vascular progenitors. (A) Experimental system for PKA activation. An embryonic stem (ES) cell line expressing constitutive active (CA) form of PKA by tetracycline-inducible expression system (Tet-Off) was established. Doxycycline (Dox) was added during the first 4.5-day culture of ES cell differentiation to Flk1$^+$ cells. Flk1$^+$ cells were sorted by magnetic cell sorting (MACS) and subjected to two-dimensional culture on collagen-coated dishes or three-dimensional culture in collagen gel, and were cultured in the presence or absence of Dox (1 μg/mL). (B-D) Two-dimensional culture with DM, at Flk-d3. (B) Double immunostaining for CD31 (purple) and αSMA (brown). (Left panel) Dox (1 μg/mL) treatment. (Right panel) Dox-free. Culture with DM alone. Scale bar represents 100 μm. (C) Flow cytometry for EC markers, CD31 and VE-cadherin. Percentages of CD31$^+$/VE-cadherin$^+$ ECs in total Flk1$^+$ cell–derived cells are indicated. (D) Fluorescent staining for CD31 (green) and DAPI (blue). (Left panels) Dox (1 μg/mL) treatment. (Right panels) Dox-free. Flk1$^+$ cells stimulated with vehicle (top panels) or VEGF (50 ng/mL; bottom panels). Scale bars represent 250 μm. (E-I) Three-dimensional culture of Flk1$^+$ cell aggregates in type I collagen gel with DM alone. (E) Phase-contrast images after 5-day culture. (Left panel) Dox (1 μg/mL) treatment. (Right panel) Dox-free. Scale bars represent 100 μm. (F) In-gel double immunostaining for CD31 (purple) and αSMA (brown) in Dox-free condition. (Left panel) Gross appearance of vascular structure. (Right panel) Higher magnification view. αSMA$^+$ cells attached to CD31$^+$ EC tube structure are observed (arrows). Scale bars represent 100 μm. (G-H) Cross-section of three-dimensional culture in Dox-free condition. (G) Hematoxylin-eosin staining. (H) Double immunostaining for CD31 (brown) and αSMA (red). Right panels correspond to boxed regions. Scale bars represent 250 μm. αSMA$^+$ cell attached to CD31$^+$ EC tube structure is observed (arrow). (I) Confocal microscopic analysis of vascular structure. Double fluorescent staining for CD31 and αSMA in Dox-free condition. (Left panel) CD31 (green). (Middle panel) αSMA (red). (Right panel) Merged image. αSMA$^+$ cell attached to CD31$^+$ EC tube structure is observed (arrow). CD31$^+$ cells formed true lumen (green) with attached mural cells (red) shown in xz image. Dashed line indicates sliced position. Scale bars represent 100 μm.

reported,[34] lower concentration of Dox (1 μg/mL) did not affect EC appearance in control ES cells (EStTA-ROSA; supplemental Figure 3). We induced differentiation of ES cells in the presence of Dox for 4.5 days, and purified Flk1$^+$ cells were recultured on type IV collagen–coated dishes with DM alone in the presence or absence of Dox (Figure 3A). In the presence of Dox (Dox$^+$), only SMA$^+$ mural cells, but not ECs were induced (Figure 3B-C), compatible with our previous results[25] (Figure 1A-B). Surprisingly, considerable amounts of CD31$^+$ ECs were generated even in the absence of VEGF when CA-PKA expression was induced by the depletion of Dox (Dox$^-$; Figure 3B; supplemental Videos 1-2). Almost all of CA-PKA–induced CD31$^+$ cells on 2-dimensional culture condition were also positive for VE-cadherin, eNOS, and claudin5 (Figure 2C, supplemental Figure 4). CD31$^-$/VE-cadherin$^-$ cells observed in CA-PKA–activated condition were positive for SMA, SM22α, and calponin (supplemental Figure 4). When we tested the effects of CA-PKA with VEGF, EC appearance with VEGF in Dox$^+$ condition was further enhanced by expression of CA-PKA (Figure 3D). These results indicate that PKA should enhance EC differentiation from vascular progenitors.

We further examined vascular formation from Flk1$^+$ cells in three-dimensional culture[25] to investigate PKA function in vascular development. When aggregates of Flk1$^+$ cells were cultured in type I collagen gel with DM alone, no sprouting of vessels was observed in Dox$^+$ condition. In contrast, CA-PKA expression (Dox$^-$) induced vascular-like structure formation even in the absence of VEGF (Figure 3E; supplemental Video 3). In-gel immunostaining showed the vascular-like structure consisted of CD31$^+$ ECs with surrounding SMA$^+$ mural cells (Figure 3F). Cross-sections revealed true lumens with CD31$^+$ ECs and attached SMA$^+$ MCs (Figure 3G-H). Confocal microscopic study further showed vascular-like structure formation with EC tube and mural cell attachment (Figure 3I). In addition, PKA activation induced CD45$^+$ blood cells within the vascular lumen (supplemental Figure 5A). Occasionally, beating cardiomyocytes, which were positive for cardiac troponin T, were observed along with vascular structures (supplemental Figure 5B; supplemental Video 4). PKA, thus, should play an important role in vascular development through enhancement of EC differentiation.

Dual up-regulation of Flk1 and NRP1 was induced by PKA

Next, we investigated the molecular mechanism of the PKA effects in EC differentiation and vascular development. First we examined PKA activity in vascular progenitor cells. Whereas PKA activity was significantly increased by addition of 8bromo-cAMP, VEGF treatment did not induce PKA activation (supplemental Figure 6),

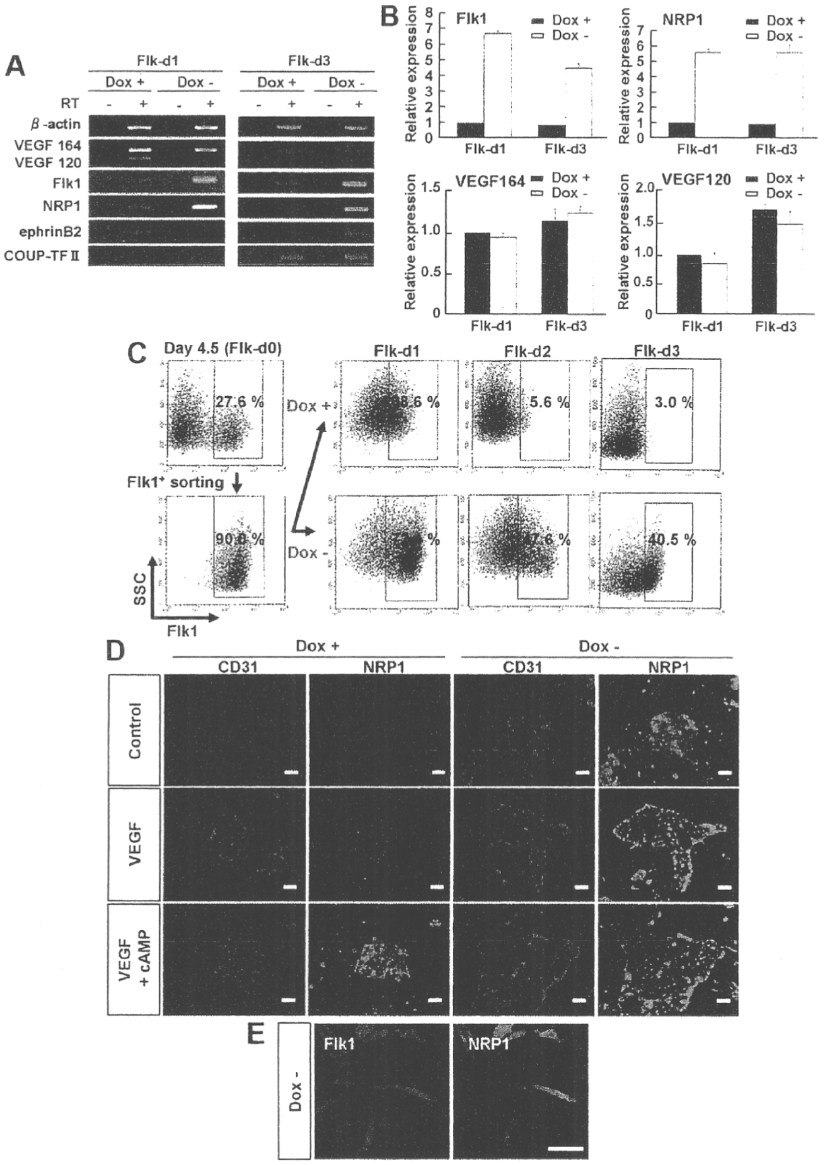

Figure 4. Dual up-regulation of Flk1 and NRP1 by PKA activation. (A-D) Two-dimensional culture of Flk1$^+$ cells. (A) RT-PCR showing mRNA expression of $VEGF_{164}$, $VEGF_{120}$, Flk1, NRP1, ephrinB2 (arterial marker), and COUP-TF II (venous marker) after 1 (Flk-d1) and 3 (Flk-d3) days of culture of Flk1$^+$ cells with DM alone in the presence or absence of Dox (1 μg/mL). (B) Quantitative RT-PCR showing mRNA expression of Flk1, NRP1, $VEGF_{164}$, and $VEGF_{120}$ at Flk-d1 and Flk-d3 in the presence or absence of Dox. mRNA expression at Flk-d1 with Dox was set as 1.0. (C) Time course of Flk1$^+$ cell appearance evaluated by FACS. Flk1$^+$ cell appearance was examined on differentiation day 4.5 before and after sorting, and at Flk-d1, Flk-d2, and Flk-d3 cultured with DM alone in the presence or absence of Dox (1 μg/mL). (Top panels) Dox treatment. (Bottom panels) Dox-free. Percentages of Flk1$^+$ cells are indicated. (D) Double fluorescent staining for CD31 and NRP1 at Flk-d3. (Left 6 panels) Dox treatment. (Right 6 panels) Dox-free. Flk1$^+$ cells stimulated with vehicle (top panels), VEGF (50 ng/mL; middle panels), or VEGF and 8bromo-cAMP (0.5 mM; bottom panels). Scale bars represent 100 μm. (E) Vascular formation from Flk1$^+$ cell aggregates in three-dimensional culture in Dox-free condition at Flk-d5. In-gel double fluorescent staining for Flk1 and NRP1. (Left panel) Flk1 (red). (Right panel) NRP1 (green). Scale bars represent 100 μm.

indicating that PKA pathway did not work downstream of VEGF signaling in vascular progenitor cells. In addition, activation of PKA by induction of CA-PKA in Flk1$^+$ cells did not increase VEGF mRNA expression (Figure 4A-B). These results indicate that PKA signaling did not enhance VEGF signaling through the formation of a positive feedback loop between VEGF and PKA. In contrast, overexpression of CA-PKA up-regulated Flk1 and NRP1 mRNA expression from the early stage of Flk1$^+$ cell culture (ie, at days 1 and 3 after Flk1 sorting; Figure 4A). Arterial EC marker, ephrinB2,[35,36] and venous EC marker, COUP-TF II,[37] were not affected by CA-PKA expression (Figure 4A). Quantitative RT-PCR analysis revealed that PKA activation induced approximately 5- to 7-fold increase in Flk1 and NRP1 mRNA expression in total cells at Flk-d1 and Flk-d3 (Figure 4B). Similar significant up-regulation of Flk1 and NRP1 mRNA expression was observed in 8bromo-cAMP–treated Flk1$^+$ cells (supplemental Figure 7A). We further confirmed the time course of Flk1 protein expression in the early stage of Flk1$^+$ cell culture by FACS. When purified Flk1$^+$ progenitor cells were cultured in the absence of VEGF, Flk1 expression was rapidly decreased and lost within 3 days, compatible with our previous results[25] (Figure 4C top panels). On the other hand, when CA-PKA was induced in purified Flk1$^+$ cells, Flk1 expression was essentially maintained, even in the absence of VEGF. At Flk-d1, almost all Flk1$^+$ cells were still negative for EC markers, CD31 and VE-cadherin (supplemental Figure 8), indicating that PKA should work at the progenitor stage to enhance EC appearance from Flk1$^+$ progenitor cells. As for NRP1 protein expression, whereas clear up-regulation of NRP1 expression was observed only in VEGF with 8bromo-cAMP treatment in Dox$^+$ condition, CA-PKA activation (Dox$^-$) induced NRP1 expression even in the absence of VEGF at Flk-d3 (Figure 4D). Furthermore, Flk1 and NRP1 were also coexpressed in vascular structure in vitro induced with CA-PKA expression (Figure 4E). These results suggest that PKA pathway should enhance EC differentiation and vascular formation through dual induction of Flk1 and NRP1.

Sensitivity of VEGF signaling is markedly enhanced by PKA

To precisely define the biologic function of up-regulated Flk1 and NRP1 by PKA activation, we tested dose-response effects of

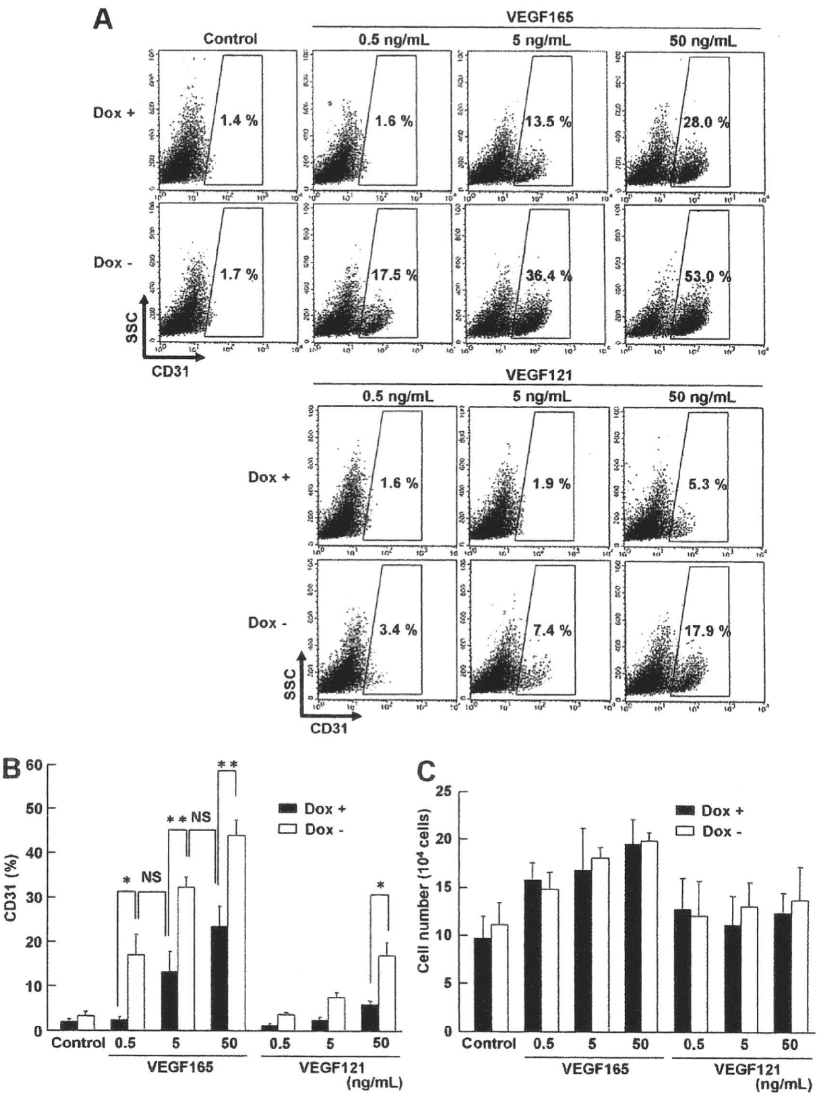

Figure 5. Sensitivity of VEGF signaling is enhanced by PKA. Serum-free culture of Flk1$^+$ cells on two-dimensional condition, at Flk-d3. (A-B) Flow cytometry for CD31 expression in the presence (Dox$^+$; 1 μg/mL) or absence (Dox$^-$) of Dox. x-axis: CD31; y-axis: SSC. Flk1$^+$ cells were incubated with various concentrations of $VEGF_{165}$ or $VEGF_{121}$ in serum-free medium, SFO3. Percentages of CD31$^+$ ECs in total Flk1$^+$ cell–derived cells are indicated. (B) Quantitative evaluation of effects of PKA activation on EC differentiation. Percentages of CD31$^+$ EC population in total Flk1$^+$ cell–derived cells are evaluated (n = 3; $^*P < .05$, $^{**}P < .01$ vs corresponding values; NS indicates not significant). (C) Quantitative evaluation of the number of induced ECs. Total cell number that appeared from 12.5×10^4 of plated Flk1$^+$ cells at Flk-d3 is shown.

$VEGF_{165}$ and $VEGF_{121}$ on Flk1$^+$ cells using serum-free culture with a defined medium, SFO3 (including insulin, transferrin, sodium selenite, and ethanolamine).[25] In the serum-free condition, CD31$^+$ ECs were not induced from Flk1$^+$ progenitors in the absence of $VEGF_{165}$. In the control condition (Dox$^+$), 5 to 50 ng/mL $VEGF_{165}$ induced CD31$^+$ ECs. Surprisingly, although almost no ECs were induced in the absence of $VEGF_{165}$ even with CA-PKA activation (Dox$^-$), CA-PKA expression induced distinct EC appearance in much lower concentration of $VEGF_{165}$ (ie, 0.5-5 ng/mL; Figure 5A-B). Similar or higher amounts of ECs were induced by 10 times lower concentration of $VEGF_{165}$ in Dox$^-$ condition compared with those in Dox$^+$ condition (CD31$^+$ cells: 18.1% ± 5.1% [Dox$^-$, 0.5 ng/mL $VEGF_{165}$] vs 14.2% ± 4.8% [Dox$^+$, 5 ng/mL $VEGF_{165}$]; 34.6% ± 2.4% [Dox$^-$, 5 ng/mL $VEGF_{165}$] vs 25.2% ± 4.8% [Dox$^+$, 50 ng/mL $VEGF_{165}$]; Figure 5B). There was no difference observed in the total cell number that appeared from Flk1$^+$ cells between Dox$^+$ and Dox$^-$ treatment (Figure 5C), suggesting that PKA activation should enhance EC differentiation but not proliferation. Furthermore, the potent enhancement of EC differentiation was observed specifically by $VEGF_{165}$ treatment, and not by $VEGF_{121}$, which does not bind to NRP1 (Figure 5A).[20] Significant increase in EC appearance with 50 ng/mL $VEGF_{121}$ (Figure 5B) should be induced by binding of $VEGF_{121}$ to up-regulated Flk1. Similarly, addition of 8bromo-cAMP in Dox$^+$ condition also enhanced response of Flk1$^+$ progenitor differentiation to VEGF (supplemental Figure 9). These results indicate that dual activation of Flk1 and NRP1 by PKA activation markedly enhanced sensitivity of Flk1$^+$ progenitors to $VEGF_{165}$.

PKA activation induces Flk1-VEGF-NRP1 complex formation

Finally, we confirmed the formation and function of Flk1-$VEGF_{165}$-NRP1 complex by PKA activation. One day after Flk1$^+$ cell culture in serum-free conditions (Flk-d1), cells were collected and protein interaction of Flk1, NRP1, and VEGF was examined by immunoprecipitation assay.[31] Western blot analysis for NRP1 using total cell lysates clearly revealed increase in NRP1 protein by CA-PKA expression (Dox$^-$) at Flk-d1 (Figure 6Aii). Total NRP1 expression was increased approximately 4.3-fold by PKA activation (n = 6; $P < .001$). In various conditions that we tested, only when added together with CA-PKA expression (Dox$^-$), $VEGF_{165}$ formed a distinct protein complex with Flk1 and NRP1 (Figure 6Ai lane 7). The protein complex was not formed in the control conditions (Dox$^+$) or Dox$^-$ conditions with the addition of $VEGF_{121}$. Similarly,

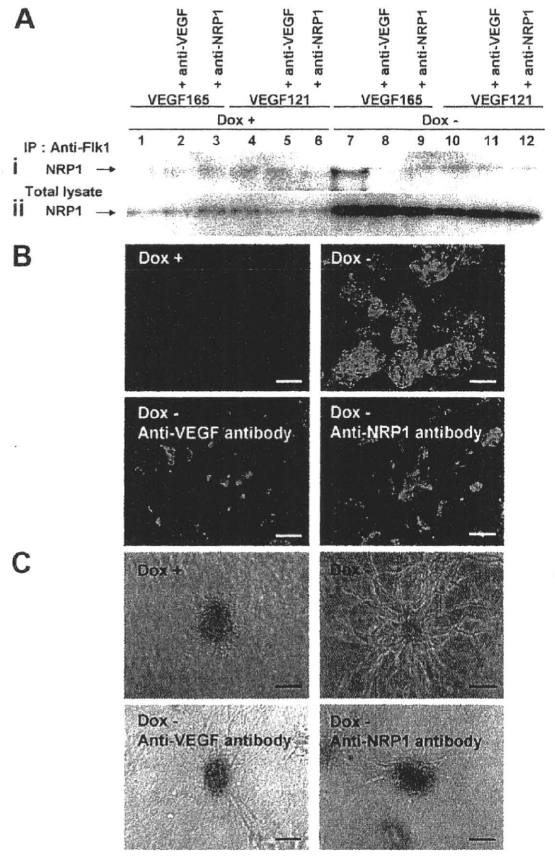

Figure 6. PKA enhanced to form Flk1-VEGF-NRP1 complexes. (A) Immunoprecipitation assay. Formation of Flk1-VEGF-NRP1 complex was examined at Flk-d1 cultured with serum-free medium, SFO3. Immunoblot with anti-NRP1 antibody for cell lysates immunoprecipitated with anti-Flk1 antibody (Ai) and total cell lysates (Aii). (Ai) Note that a distinct band was observed only when $VEGF_{165}$ was added to PKA-activated (Dox^-) condition (lane 7), which was inhibited by addition of anti-VEGF or anti-NRP1 antibodies. (Aii) Total NRP1 expression was markedly increased in PKA-activated condition. (B) Two-dimensional culture of $Flk1^+$ cells with DM, at Flk-d3. Fluorescent staining for CD31 (green). Nuclei are stained with DAPI (blue). (Top left panel) Dox treatment. (Other panels) Dox-free. (Bottom left panel) Dox-free with neutralizing antibody for VEGF. (Bottom right panel) Dox-free with neutralizing antibody for NRP1. Scale bars represent 250 μm. (C) Vascular formation from $Flk1^+$ cell aggregates in three-dimensional culture. (Top left panel) Dox treatment. (Other panels) Dox-free. (Bottom left panel) Dox-free with neutralizing antibody for VEGF. (Bottom right panel) Dox-free with neutralizing antibody for NRP1. Scale bars represent 100 μm.

8bromo-cAMP treatment also induced formation of a protein complex with Flk1, NRP1, and $VEGF_{165}$ (supplemental Figure 7B). These results clearly indicated that PKA activation induced both Flk1 and NRP1 expression in vascular progenitors, and $VEGF_{165}$ in turn specifically induced the protein complex formation of Flk1-$VEGF_{165}$-NRP1. The formation of Flk1-$VEGF_{165}$-NRP1 complex was completely blocked by the addition of anti-VEGF or anti-NRP1 neutralizing antibodies (Figure 6Ai lanes 8-9). Parallel to the Flk1-$VEGF_{165}$-NRP1 complex formation, the CA-PKA–induced EC differentiation as well as vascular formation in three-dimensional culture were drastically inhibited by the addition of anti-VEGF or NRP1 neutralizing antibodies, suggesting a functional significance of the Flk1-$VEGF_{165}$-NRP1 complex (Figure 6B-C). These results indicate that PKA regulates sensitivity of vascular progenitors to VEGF by dual induction of Flk1 and NRP1, which forms the Flk1-$VEGF_{165}$-NRP1 complex enhancing VEGF signaling to efficiently induce EC differentiation and vascular formation.

Discussion

Here, we showed a novel regulatory mechanism of EC differentiation and vascular formation through the modulation of progenitor properties to be endothelial competent. PKA activation increased both Flk1 and NRP1 expression in vascular progenitors and markedly enhanced the "sensitivity" of the progenitors to $VEGF_{165}$ by inducing Flk1-$VEGF_{165}$-NRP1 complex formation. This new-mode regulatory system would provide insights in vascular development and offer options for various therapeutic strategies with vascular manipulation.

Vascular formation is regulated by appropriate intensity, space, and timing of VEGF signaling. This study showed that PKA is involved in vascular formation process through its novel function regulating VEGF signal intensity. Various factors, such as adrenomedullin,[38] prostaglandins,[39] adiponectin,[40] ghrelin,[41] klotho,[42] and mechanical stress, especially fluid shear stress,[43] have been reported to activate PKA in ECs. We previously demonstrated that adrenomedullin could enhance EC differentiation from $Flk1^+$ cells through cAMP signaling.[26] Fluid shear stress was reported to enhance EC differentiation from $Flk1^+$ cells by up-regulating VEGF receptors,[44] and to induce Flk1 gene expression in EC cell lines.[45] These multiple PKA-activating signals should be involved in vascular development to modulate the progenitor sensitivity in vivo.

We previously reported that adrenomedullin/cAMP pathway induced differentiation of arterial ECs.[26] We also examined involvement of PKA in arterial-venous specification. Whereas addition of PKI, PKA inhibitor, to $Flk1^+$ cell culture with VEGF and 8bromo-cAMP significantly decreased total $CD31^+$ EC appearance (Figure 2A-D), PKI did not inhibit ephrinB2- or CXCR4-positive arterial EC differentiation (supplemental Figure 10). Moreover, expression of CA-PKA with VEGF did not induce arterial ECs from $Flk1^+$ vascular progenitors (supplemental Figure 11). These results indicated that PKA is not involved in arterial-venous specification. Activation of PKA in $Flk1^+$ cells did not induce prox1- or podoplanin-positive lymphatic ECs (supplemental Figure 11), further suggesting that PKA pathway is involved in common EC differentiation but not in EC specification processes.

Some studies have reported the roles of downstream molecules of Flk1 signaling in EC proliferation and differentiation. Tyrosine residue 1173 of Flk1 (Y1173, corresponding to Y1175 in human Flk1, KDR) is essential for Flk1 function in vasculogenesis.[46] Y1175 of KDR is a binding site of PLCγ and is important for VEGF-dependent EC proliferation.[47] Furthermore, Ras signaling acting downstream of Flk1 signaling plays a critical role in EC differentiation.[32] Indeed, PLC inhibitor, U73122, or H-Ras inhibitor, FTI-277, showed an inhibitory effect on EC differentiation from $Flk1^+$ cells (supplemental Figure 12), indicating that PLC and Ras pathway are both downstream molecules of Flk1 signaling. Enhanced VEGF signaling in vascular progenitors by PKA should be mediated by these molecules to induce basal EC differentiation.

Molecular mechanisms of PKA to induce and/or maintain Flk1 and NRP1 expression in vascular progenitors are largely unknown. NRP1 expression was reported to be up-regulated by cAMP/PKA pathway in olfactory neuron guidance.[48] Some other reports have shown that PKA pathway enhances differentiation of neuronal progenitor cells,[49] hippocampal progenitor cells,[50] and oligodendrocyte progenitor cells.[51] Recently, evidence is accumulating to suggest that blood vessels and nerves share a similar molecular machinery to form their networks.[52] Blood vessels and nerves may use PKA as common regulatory cues for their differentiation and

development. Further elucidation of molecular interaction among PKA, Flk1, and NRP1 should provide a novel molecular framework for tissue development.

Very recently, Cimato et al reported that NRP1 was largely coexpressed with Flk1 to identify endothelial precursors in human and mouse ES cells.[53] We confirmed that low-level expression of NRP1 was observed in Flk1$^+$ progenitors and was increased in ECs (supplemental Figure 13). These 2 functional markers for EC progenitors, Flk1 and NRP1, were, thus, commonly regulated by PKA to efficiently enhance their progenitor potentials responding to VEGF signaling.

We have succeeded in uncovering novel roles of PKA in EC differentiation and vascular development using our unique ES cell differentiation system. Elucidation of the new-mode cell fate determination mechanisms by modulation of progenitor potentials would provide novel insights in developmental biology, stem cell biology, and regenerative medicine.

Acknowledgments

We are grateful to Dr T. Era (Kumamoto University) for EStTA5-4 cells, to G. S. McKnight (University of Washington School of Medicine) for the CA-PKA plasmid, K. Tanimoto (University of Tsukuba) and P. Soriano (Mt Sinai School of Medicine) for the loxP knockin vector for ROSA locus, and Y. Toda for three-dimensional histologic analyses. We thank M. Takahashi for critical reading of the paper.

This study was supported by grants from the Ministry of Education, Science, Sports and Culture of Japan, the Ministry of Health, Labor and Welfare, the New Energy and Industrial Development Organization (NEDO) of Japan, and the Project for Realization of Regenerative Medicine.

Authorship

Contribution: K.Y. performed all experiments and wrote the paper; K.K. and T.W. performed ex vivo whole-embryo experiments; S.K. helped with immunostaining experiments; and J.K.Y. supervised all experiments and wrote the paper.

Conflict-of-interest disclosure: The authors declare no competing financial interests.

Correspondence: Jun K. Yamashita, Laboratory of Stem Cell Differentiation, Stem Cell Research Center, Institute for Frontier Medical Sciences, Kyoto University, 53 Shogoin Kawahara-cho, Sakyo-ku, Kyoto 606-8507 Japan; e-mail: juny@frontier.kyoto-u.ac.jp.

References

1. Coultas L, Chawengsaksophak K, Rossant J. Endothelial cells and VEGF in vascular development. *Nature.* 2005;438(7070):937-945.
2. Carmeliet P, Jain RK. Angiogenesis in cancer and other diseases. *Nature.* 2000;407(6801):249-257.
3. Ferrara N. Vascular endothelial growth factor: basic science and clinical progress. *Endocr Rev.* 2004;25(4):581-611.
4. Shibuya M. Differential roles of vascular endothelial growth factor receptor-1 and receptor-2 in angiogenesis. *J Biochem Mol Biol.* 2006;39(5):469-478.
5. Hanahan D. Signaling vascular morphogenesis and maintenance. *Science.* 1997;277(5322):48-50.
6. Seetharam L, Gotoh N, Maru Y, Neufeld G, Yamaguchi S, Shibuya M. A unique signal transduction from FLT tyrosine kinase, a receptor for vascular endothelial growth factor VEGF. *Oncogene.* 1995;10(1):135-147.
7. Waltenberger J, Claesson-Welsh L, Siegbahn A, Shibuya M, Heldin CH. Different signal transduction properties of KDR and Flt1, two receptors for vascular endothelial growth factor. *J Biol Chem.* 1994;269(43):26988-26995.
8. Millauer B, Wizigmann-Voos S, Schnürch H, et al. High affinity VEGF binding and developmental expression suggest Flk-1 as a major regulator of vasculogenesis and angiogenesis. *Cell.* 1993;72(6):835-846.
9. Shalaby F, Rossant J, Yamaguchi TP, et al. Failure of blood-island formation and vasculogenesis in Flk-1-deficient mice. *Nature.* 1995;376(6535):62-66.
10. Fong GH, Rossant J, Gertsenstein M, Breitman ML. Role of the Flt-1 receptor tyrosine kinase in regulating the assembly of vascular endothelium. *Nature.* 1995;376(6535):66-70.
11. Fong GH, Zhang L, Bryce DM, Peng J. Increased hemangioblast commitment, not vascular disorganization, is the primary defect in flt-1 knock-out mice. *Development.* 1999;126(13):3015-3025.
12. Hiratsuka S, Minowa O, Kuno J, Noda T, Shibuya M. Flt-1 lacking the tyrosine kinase domain is sufficient for normal development and angiogenesis in mice. *Proc Natl Acad Sci U S A.* 1998;95(16):9349-9354.
13. Carmeliet P, Ferreira V, Breier G, et al. Abnormal blood vessel development and lethality in embryos lacking a single VEGF allele. *Nature.* 1996;380(6573):435-439.
14. Miquerol L, Langille BL, Nagy A. Embryonic development is disrupted by modest increases in vascular endothelial growth factor gene expression. *Development.* 2000;127(18):3941-3946.
15. Kitsukawa T, Shimono A, Kawakami A, Kondoh H, Fujisawa H. Overexpression of a membrane protein, neuropilin, in chimeric mice causes anomalies in the cardiovascular system, nervous system and limbs. *Development.* 1995;121(12):4309-4318.
16. Kawakami A, Kitsukawa T, Takagi S, Fujisawa H. Developmentally regulated expression of a cell surface protein, neuropilin, in the mouse nervous system. *J Neurobiol.* 1996;29(1):1-17.
17. He Z, Tessier-Lavigne M. Neuropilin is a receptor for the axonal chemorepellent Semaphorin III. *Cell.* 1997;90(4):739-751.
18. Kolodkin AL, Levengood DV, Rowe EG, Tai YT, Giger RJ, Ginty DD. Neuropilin is a semaphorin III receptor. *Cell.* 1997;90(4):753-762.
19. Geretti E, Shimizu A, Klagsbrun M. Neuropilin structure governs VEGF and semaphorin binding and regulates angiogenesis. *Angiogenesis.* 2008;11(1):31-39.
20. Soker S, Takashima S, Miao HQ, Neufeld G, Klagsbrun M. Neuropilin-1 is expressed by endothelial and tumor cells as an isoform-specific receptor for vascular endothelial growth factor. *Cell.* 1998;92(6):735-745.
21. Yamaguchi TP, Dumont DJ, Conlon RA, Breitman MLRossant J. flk-1, an flt-related receptor tyrosine kinase is an early marker for endothelial cell precursors. *Development.* 1993;118(2):489-498.
22. Eichmann A, Corbel C, Nataf V, Vaigot P, Bréant C, Le Douarin NM. Ligand-dependent development of the endothelial and hemopoietic lineages from embryonic mesodermal cells expressing vascular endothelial growth factor receptor 2. *Proc Natl Acad Sci U S A.* 1997;94(10):5141-5146.
23. Kennedy M, Firpo M, Choi K, et al. A common precursor for primitive erythropoiesis and definitive haematopoiesis. *Nature.* 1997;386(6624):488-493.
24. Nishikawa SI, Nishikawa S, Hirashima M, Matsuyoshi N, Kodama H. Progressive lineage analysis by cell sorting and culture identifies FLK1+VE-cadherin+ cells at a diverging point of endothelial and hemopoietic lineages. *Development.* 1998;125(9):1747-1757.
25. Yamashita J, Itoh H, Hirashima M, et al. Flk1-positive cells derived from embryonic stem cells serve as vascular progenitors. *Nature.* 2000;408(6808):92-96.
26. Yurugi-Kobayashi T, Itoh H, Schroeder T, et al. Adrenomedullin/cyclic AMP pathway induces Notch activation and differentiation of arterial endothelial cells from vascular progenitors. *Arterioscler Thromb Vasc Biol.* 2006;26(9):1977-1984.
27. Era T, Witte ON. Regulated expression of P210 Bcr-Abl during embryonic stem cell differentiation stimulates multipotential progenitor expansion and myeloid cell fate. *Proc Natl Acad Sci U S A.* 2000;97(4):1737-1742.
28. Zambrowicz BP, Imamoto A, Fiering S, Herzenberg LA, Kerr WG, Soriano P. Disruption of overlapping transcripts in the ROSA beta geo 26 gene trap strain leads to widespread expression of beta-galactosidase in mouse embryos and hematopoietic cells. *Proc Natl Acad Sci U S A.* 1997;94(8):3789-3794.
29. Orellana SA, McKnight GS. Mutations in the catalytic subunit of cAMP-dependent protein kinase result in unregulated biological activity. *Proc Natl Acad Sci U S A.* 1992;89(10):4726-4730.
30. Toda Y, Kono K, Abiru H, et al. Application of tyramide signal amplification system to immunohistochemistry: a potent method to localize antigens that are not detectable by ordinary method. *Pathol Int.* 1999;49(5):479-483.
31. Pan Q, Chathery Y, Wu Y, et al. Neuropilin-1 binds to VEGF121 and regulates endothelial cell migration and sprouting. *J Biol Chem.* 2007;282(33):24049-24056.
32. Kawasaki K, Watabe T, Sase H, et al. Ras signaling directs endothelial specification of VEGFR2+ vascular progenitor cells. *J Cell Biol.* 2008;181(1):131-141.

33. Hogan B, Beddington R, Constantini F, Lacy E. *Manipulating the Mouse Embryo: A Laboratory Manual*. Cold Spring, New York: Cold Spring Harbor Laboratory Press; 1994.

34. Gilbertson-Beadling S, Powers EA, Stamp-Cole M, et al. The tetracycline analogs minocycline and doxycycline inhibit angiogenesis in vitro by a non-metalloproteinase-dependent mechanism. *Cancer Chemother Pharmacol*. 1995;36(5):418-424.

35. Wang HU, Chen ZF, Anderson DJ. Molecular distinction and angiogenic interaction between embryonic arteries and veins revealed by ephrin-B2 and its receptor Eph-B4. *Cell*. 1998;93(5):741-753.

36. Adams RH, Wilkinson GA, Weiss C, et al. Roles of ephrinB ligands and EphB receptors in cardiovascular development: demarcation of arterial/venous domains, vascular morphogenesis, and sprouting angiogenesis. *Genes Dev*. 1999;13(3):295-306.

37. You LR, Lin FJ, Lee CT, DeMayo FJ, Tsai MJ, Tsai SY. Suppression of Notch signalling by the COUP-TFII transcription factor regulates vein identity. *Nature*. 2005;435(7038):98-104.

38. Miyashita K, Itoh H, Sawada N, et al. Adrenomedullin promotes proliferation and migration of cultured endothelial cells. *Hypertens Res*. 2003;26:S93-S98.

39. Birukova AA, Zagranichnaya T, Fu P, et al. Prostaglandins PGE(2) and PGI(2) promote endothelial barrier enhancement via PKA- and Epac1/Rap1-dependent Rac activation. *Exp Cell Res*. 2007;313(11):2504-2520.

40. Ouchi N, Kihara S, Arita Y, et al. Adiponectin, an adipocyte-derived plasma protein, inhibits endothelial NF-kappaB signaling through a cAMP-dependent pathway. *Circulation*. 2000;102(11):1296-1301.

41. Rossi F, Bertone C, Petricca S, Santiemma V. Ghrelin inhibits angiotensin II-induced migration of human aortic endothelial cells. *Atherosclerosis*. 2007;192(2):291-297.

42. Yang J, Matsukawa N, Rakugi H, et al. Upregulation of cAMP is a new functional signal pathway of Klotho in endothelial cells. *Biochem Biophys Res Commun*. 2003;301(2):424-429.

43. Csiszar A, Labinskyy N, Smith KE, et al. Downregulation of bone morphogenetic protein 4 expression in coronary arterial endothelial cells: role of shear stress and the cAMP/protein kinase A pathway. *Arterioscler Thromb Vasc Biol*. 2007;27(4):776-782.

44. Yamamoto K, Sokabe T, Watabe T, et al. Fluid shear stress induces differentiation of Flk-1-positive embryonic stem cells into vascular endothelial cells in vitro. *Am J Physiol Heart Circ Physiol*. 2005;288(4):H1915-H1924.

45. Urbich C, Stein M, Reisinger K, Kaufmann R, Dimmeler S, Gille J. Fluid shear stress-induced transcriptional activation of the vascular endothelial growth factor receptor-2 gene requires Sp1-dependent DNA binding. *FEBS Lett*. 2003;535(1-3):87-93.

46. Sakurai Y, Ohgimoto K, Kataoka Y, Yoshida N, Shibuya M. Essential role of Flk-1 (VEGF receptor 2) tyrosine residue 1173 in vasculogenesis in mice. *Proc Natl Acad Sci U S A*. 2005;102(4):1076-81.

47. Takahashi T, Yamaguchi S, Chida K, Shibuya M. A single autophosphorylation site on KDR/Flk-1 is essential for VEGF-A-dependent activation of PLC-gamma and DNA synthesis in vascular endothelial cells. *EMBO J*. 2001;20(11):2768-2778.

48. Imai T, Suzuki M, Sakano H. Odorant receptor-derived cAMP signals direct axonal targeting. *Science*. 2006;314(5799):657-661.

49. Vogt Weisenhorn DM, Roback LJ, Kwon JH, Wainer BH. Coupling of cAMP/PKA and MAPK signaling in neuronal cells is dependent on developmental stage. *Exp Neurol*. 2001;169(1):44-55.

50. Kim G, Choe Y, Park J, Cho S, Kim K. Activation of protein kinase A induces neuronal differentiation of HiB5 hippocampal progenitor cells. *Brain Res Mol Brain Res*. 2002;109(1-2):134-145.

51. Shiga H, Asou H, Ito E. Advancement of differentiation of oligodendrocyte progenitor cells by a cascade including protein kinase A and cyclic AMP-response element binding protein. *Neurosci Res*. 2005;53(4):436-441.

52. Carmeliet P, Tessier-Lavigne M. Common mechanisms of nerve and blood vessel wiring. *Nature*. 2005;436(7048):193-200.

53. Cimato T, Beers J, Ding S, et al. Neuropilin-1 identifies endothelial precursors in human and murine embryonic stem cells before CD34 expression. *Circulation*. 2009;119(16):2170-2178.

Cardiovascular Research (2009) 83, 682–687
doi:10.1093/cvr/cvp171

The cardiac pacemaker-specific channel *Hcn4* is a direct transcriptional target of MEF2

Shinobu Kuratomi[1], Yoko Ohmori[1], Masayuki Ito[1], Kuniko Shimazaki[1], Shin-ichi Muramatsu[2], Hiroaki Mizukami[3], Hideki Uosaki[4], Jun K. Yamashita[4], Yuji Arai[5], Koichiro Kuwahara[6], and Makoto Takano[1]*

[1]*Department of Physiology, School of Medicine, Jichi Medical University, Shimotsuke, Tochigi 329-0498, Japan;* [2]*Division of Neurology, Department of Medicine, School of Medicine, Jichi Medical University, Shimotsuke, Tochigi 329-0498, Japan;* [3]*Division of Genetic Therapeutics, Center for Molecular Medicine, Jichi Medical University, Shimotsuke, Tochigi 329-0498, Japan;* [4]*Laboratory of Stem Cell Differentiation, Stem Cell Research Center, Institute for Frontier Medical Sciences, Kyoto University, Kyoto 606-8507, Japan;* [5]*Department of Bioscience, National Cardiovascular Center Research Institute, Suita, Osaka 565-8565, Japan; and* [6]*Department of Medicine and Clinical Sciences, Graduate School of Medicine, Kyoto University, Kyoto 606-8507, Japan*

Received 21 January 2009; revised 8 May 2009; accepted 22 May 2009; online publish-ahead-of-print 28 May 2009

Time for primary review: 34 days

KEYWORDS
Hcn4;
MEF2;
Sino-atrial node;
Channel;
Transcription

Aims *Hcn4*, which encodes the hyperpolarization-activated, cyclic nucleotide-sensitive channel (I_h), is a well-established marker of the cardiac sino-atrial node. We aimed to identify *cis*-elements in the genomic locus of the *Hcn4* gene that regulate the transcription of *Hcn4*.

Methods and results We screened evolutionarily conserved non-coding sequences (CNSs) that are often involved in the regulation of gene expression. The VISTA Enhancer Browser identified 16 regions, termed CNS 1-16, within the *Hcn4* locus. Using the luciferase reporter assay in primary neonatal rat cardiomyocytes, we found that CNS13 conferred a prominent enhancer activity (more than 30-fold) on the *Hcn4* promoter. Subsequent mutation analysis revealed that the *Hcn4* enhancer function was dependent on myocyte enhancer factor-2 (MEF2) and activator protein-1 (AP1) binding sequences located in CNS13. Electrophoretic mobility shift assay and chromatin immunoprecipitation confirmed that MEF2 and AP1 proteins bound CNS13. Furthermore, overexpression of a dominant negative MEF2 mutant inhibited the enhancer activity of CNS13, decreased *Hcn4* mRNA expression and also decreased the amplitude of I_h current in myocytes isolated from the inflow tract of embryonic heart.

Conclusion These results suggest that the novel enhancer CNS13 and MEF2 may play a critical role in the transcription of *Hcn4* in the heart.

1. Introduction

The appropriate timing of cardiac muscle contraction is regulated by the electrical conduction system of the heart and consists of cardiomyocytes possessing specialized electrical function. The precise expression pattern of cardiac ion channel genes in relation to such electrophysiological properties has been extensively studied.[1,2] Previous reports have demonstrated that the hyperpolarization-activated, cyclic nucleotide-sensitive cation current (I_h) encoded by the *Hcn4* gene appears one of the ion currents underlying pacemaker depolarization.[3,4] In mammalian adult heart, *Hcn4* is specifically expressed in the sino-atrial node (SAN). During development *Hcn4* is also expressed in the foetal and neonatal chamber myocardium. As a result of this distribution, *Hcn4* is now recognized as a key marker gene of the SAN.[5,6] Despite its role as an SAN marker, little is known about the *cis*-elements that directly regulate *Hcn4* expression. Progress in the genome project and comparative genomic-base approaches have proven useful in the identification of gene regulatory sequences in a wide range of genomic loci.[7,8] We have previously reported that an 847 bp proximal sequence induces minimal promoter activity of the *Hcn4* gene.[9] In addition to this proximal upstream region, we also identified conserved, non-coding sequences within the *Hcn4* gene locus and analysed their enhancer function. We found that the novel enhancer contained binding sites for activator protein-1 (AP1) and myocyte enhancer factor-2 (MEF2) and played a critical role in the expression of *Hcn4*. These results outline the potential mechanisms underlying SAN differentiation.

* Corresponding author. Tel: +81 285 58 7308; Fax: +81 285 40 6294.
E-mail address: takanom@jichi.ac.jp

2. Methods

2.1 Construction of the promoter reporter plasmid

Luciferase reporter constructs were prepared using pGL4.10 vector (Promega) and the *Hcn4* promoter construct was obtained as previously described.[9] Conserved non-coding sequence (CNS) fragments were isolated from mouse genomic DNA by PCR with the primer pairs listed in Supplementary material online, *Table S1* and were subcloned into the upstream region of the *Hcn4* promoter.

2.2 Cell culture

For the culture of neonatal cardiomyocytes, 1- to 2-day-old rats were decapitated, the ventricle rapidly dissected and myocytes isolated by collagenase digestion (Worthington, type 2, 80 U/mL). The myocytes were then enriched by discontinuous Percoll gradient centrifugation (yield more than 90%).

For the culture of embryonic cardiomyocytes, rat embryos (13 days after fertilization) were removed from pregnant rats under deep anaesthesia with ether, the inflow tract of embryonic heart dissected and the primordial right and left appendixes removed. Myocytes were then isolated using the same procedure as that for the culture of neonatal myocytes.

Embryonic and neonatal cardiomyocytes were plated at a density of 2×10^4 and 10^5 cells/well, respectively, in 24-well plates and cultured in DMEM with 10% foetal bovine serum.[9]

All experiments were approved in advance by the animal Ethics Committee of Jichi Medical University. The investigation conforms with the Guide for the Care and Use of Laboratory Animals published by the US National Institutes of Health (NIH Publication No. 85-23, revised 1996).

2.3 Luciferase reporter gene assay

Luciferase reporter constructs (0.5 μg) and pGL4.74 vector (0.03 μg) were co-transfected into neonatal cardiomyocytes using Lipofectamine LTX (Invitrogen). Luciferase activities were measured 3 days after the transfection using the Dual-Luciferase Reporter Assay System (Promega). Transcriptional activities were obtained from three separate assays performed in quadruplicate.

2.4 Electrophoretic mobility shift assays

The myc-tagged mouse c-Jun/AP1 and MEF2C proteins were *in vitro* translated using TNT Quick Coupled Transcription/Translation System (Promega) and CNS13 DNA probes radiolabelled with [^{32}P]. The binding reaction was then performed in a reaction buffer (final volume=20 μL) containing 20 mM HEPES (pH 7.6), 50 mM KCl, 1 mM $MgCl_2$, 0.1% Nonidet P-40, 5% glycerol, 5 mM dithiothreitol, 1 mM EDTA, and 1 μg poly(dI-dC). The probe (10 fmol) incubated with 1 μL of protein was analysed on 4% polyacrylamide gels in ×0.25 TBE buffer. In competition experiments, 100-fold molar excess of double-strand oligonucleotides (AP1: 5′-ATT CTG AGT CAG AGA-3′ and MEF2: 5′-AGG TGG GTT AAA AAT AGA GCC CT-3′) were added.

2.5 Chromatin immunoprecipitation

Chromatin isolated from neonatal rat cardiomyocytes was immunoprecipitated with specific antibodies directed against anti-c-Jun/AP1 (Calbiochem) and anti-MEF2 (AnaSpec) using the EZ chromatin immunoprecipitation (ChIP) assay kit (Upstate) and analysed by PCR using the following primer pairs: CNS13 ChIP primers 5′-CCT TGG TTG TGA GTC TGT GTC T-3′ (forward) and 5′-AGT GGA GAG ACT GCT CTT TTC C-3′ (reverse) and control ChIP primers 5′-AAT GGG ACT CCT CTT ACT CAT TTC T-3′ (forward) and 5′-AAA GTC CCT GAT GAC ACA CTA GTT C-3′ (reverse).

2.6 AAV vector production and transfection

Adeno-associated virus (AAV) vector plasmids contain an expression cassette consisting of a CMV promoter followed by the first intron of human growth hormone, target cDNA, woodchuck hepatitis virus post-transcriptional regulatory element (GenBank accession no. J04514) and the SV40 poly-A signal sequence, between the inverted terminal repeats of the AAV-3 genome. The plasmids pAAV-dnMEF2 and pAAV-GFP contained the cDNA of the dominant negative MEF2 (dnMEF2) fused with Orange fluorescent protein (Clontech) and GFP, respectively. The two helper plasmids, pHelper (Agilent) and pAAV1-RC, harbour the *E2A*, *E4*, and *VA RNA* genes of the adenovirus genome, and the AAV-1 *rep* and *cap* genes, respectively. HEK293 cells were cotransfected using the calcium phosphate coprecipitation method with the vector plasmid, pAAV1-RC and pHelper. AAV1 vectors were harvested and purified via two sequential continuous iodoxale ultracentrifugations. The vector titer was determined by quantitative PCR (Q-PCR) of DNase I-treated vector stocks, yielding 10^{11}–10^{12} vector genome copies (vg).[12] 2×10^4 foetal myocytes were transfected with 10^{10} vg AAV1-dnMEF2 or AAV1-EGFP; and 10^5 vg Empty AV5 vector was also transfected as a helper.

2.7 RT-PCR and Q-PCR analysis

Three days after the transfection of AAV1, total RNA was isolated from primary cultured embryonic myocytes using TRIZOL reagent (Invitrogen). Single-strand cDNA was synthesized using Superscript III (Invitrogen). Q-PCR was carried out with predesigned Taqman Probes for *hcn4*, *hcn2*, *hcn1*, *stars*, and the 18s rRNA, in an ABI Prism 7700 System (Applied Biosystems).

2.8 Immunostaining of cardiomyocytes

Cardiomyocytes were fixed with 4% paraformaldehyde and incubated with primary antibodies directed against HCN4 (1:200 dilution; Chemicon) and actinin (1:750; Monoclonal, Sigma). Following extensive washes, cells were incubated with Alexa Fluor 488-conjugated anti-rabbit or anti-mouse Ig secondary antibodies at a concentration of 1:500 (Molecular Probes).

2.9 Electrophysiological analysis

Electrophysiological measurements were carried out using an Axopatch200B amplifier and a Digidata 1320 interface (Axon). The bathing solution contained 140 mM NaCl, 5.4 mM KCl, 0.33 mM NaH_2PO_4, 0.5 mM $MgCl_2$, 1.8 mM $CaCl_2$, 0.5 mM $BaCl_2$, 5 mM HEPES (pH 7.4 with NaOH), and the standard high K^+ pipette solution contained 110 Aspartic acid, 30 mM KCl, 5 mM MgATP, 5 mM Na_2 creatine phosphate, 0.1 mM Na_2GTP, 2 mM EGTA, 10 mM HEPES (pH 7.2 with KOH).

2.10 Statistical analysis

Data are expressed as mean ± SD values. Statistical analysis was performed using the Student's *t*-test and $P < 0.05$ was defined as statistically significant.

3. Results

3.1 Functional analysis of conserved non-coding regions within the *Hcn4* gene locus

Our previous study revealed that the proximal 847 bp sequence in the *Hcn4* upstream region is essential for promoter activity.[9] In order to locate additional *cis*-regulatory sequences, we extensively searched the CNSs in the genomic locus of *Hcn4*. As illustrated in *Figure 1A*, we identified 16 regions using VISTA Enhancer Browser, and designated these regions CNS 1-16 (Supplementary material online, *Table S1*).[8]

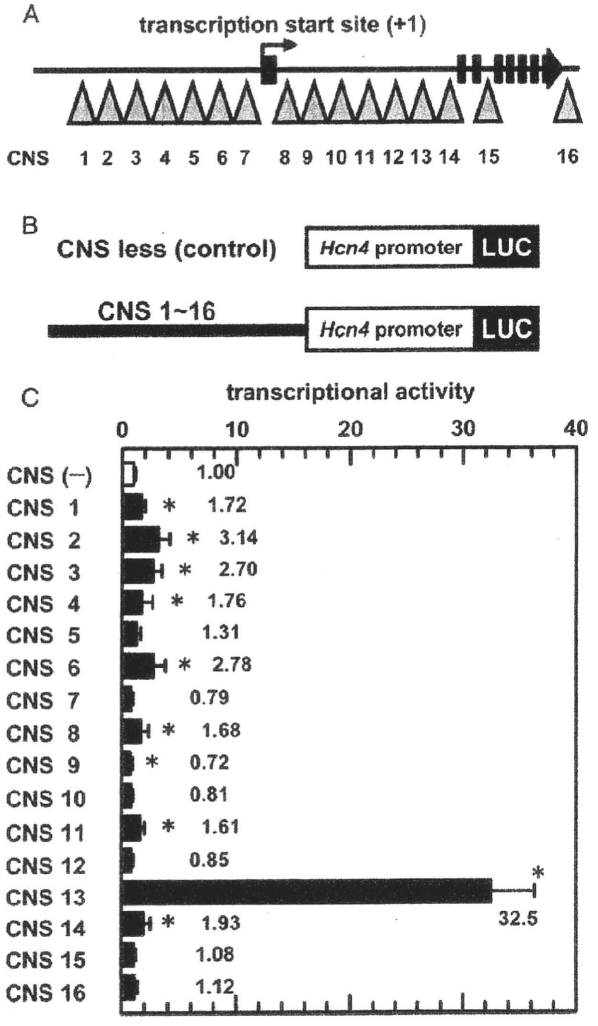

Figure 1 Enhancer activity of the CNS fragments. (*A*) A schematic diagram outlining the genomic organization of the murine *Hcn4* gene. Arrows indicate CNS regions. (*B*) Structure of the luciferase reporter constructs. The *Hcn4* promoter comprises nucleotides −446 to +400 relative to the transcription start site. (*C*) Enhancer activity conferred by the CNS fragments. Data are presented as relative values to the activity of the *Hcn4* promoter. $^*P < 0.05$ compared with construct of *Hcn4* promoter alone.

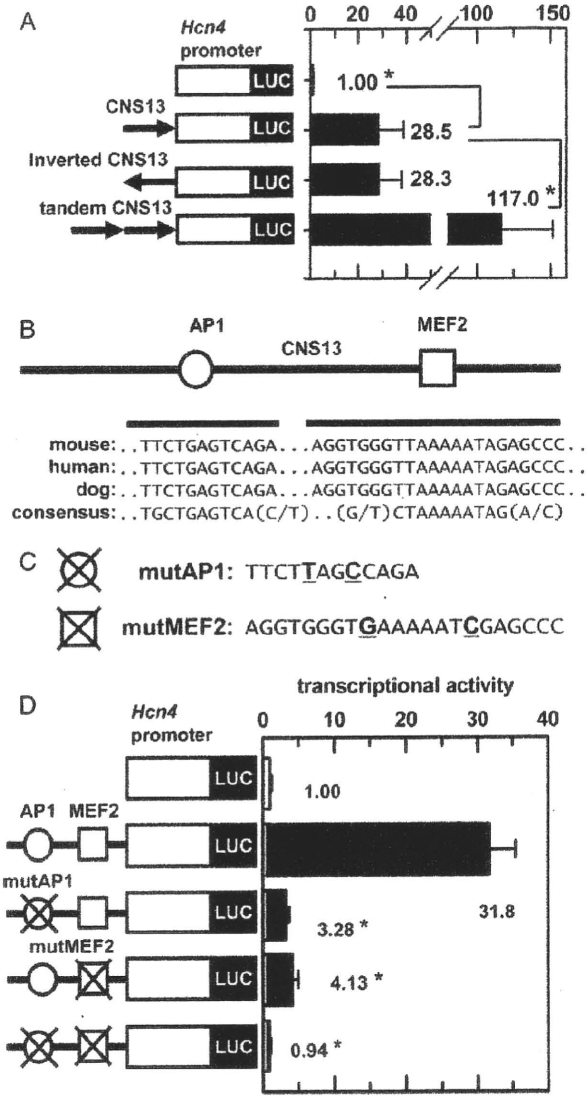

Figure 2 MEF2 and AP1 sites are essential in CNS13. (*A*) A schematic diagram of control, inverted, and tandem CNS13 constructs. The inverted construct was made by swapping the restriction sites at the ends of the control CNS13 fragment. The tandem construct, by introducing *Eco*RI site between the fragments. $^*P < 0.05$ compared with control CNS13 construct. (*B*) A schematic diagram of the putative binding sequences for AP1 (open circle) and MEF2 (open square) in CNS13. The AP1 and MEF2 sequences in mouse, human, and dog are aligned with the consensus sequences. The score for the matches were AP1: core match 1.000; matrix match 0.923. MEF2: core match 1.000; matrix match 0.957. (*C*) Mutation of the AP1 and MEF2 sites. The bold, underlined characters indicate the substituted nucleotides. (*D*) Enhancer activity of the CNS13 mutants. Data is presented as relative values to the activity of the *Hcn4* promoter. $^*P < 0.05$ compared with *Hcn4* promoter.

We next evaluated enhancer activity for each of the CNS regions using the luciferase reporter assay. In order to achieve this, we linked CNS fragments to the *Hcn4* promoter expressing the luciferase reporter gene in the pGL4.10 vector (*Figure 1B*) and analysed enhancer function in cultured primary cardiomyocytes. As shown in *Figure 1C*, nine CNS fragments (CNS1, 2, 3, 4, 6, 8, 11, 13, and 14) significantly enhanced *Hcn4* promoter activity. The CNS13 construct led to an ~33-fold increase in transcriptional activity, in comparison to the remainder of the constructs that resulted in no more than a 3.2-fold increase.

3.2 MEF2 and AP1 sites are required for the enhancer activity of CNS13

To confirm that CNS13 acts as an authentic enhancer, we next constructed inverted CNS13 and tandem repeated CNS13 fragments and fused with the *Hcn4* promoter. As shown in *Figure 2A*, no significant difference was found between the enhancer activities of normal- and inverted-CNS13 fragments. Tandem repeat CNS13 robustly activated the *Hcn4* promoter. We then focused our study on the CNS13 sequence and explored its *cis*-regulatory mechanism and its potential as a novel enhancer for the *Hcn4* promoter.

To characterize functional motifs in the CNS13 sequence, we searched putative transcription factor binding sites using

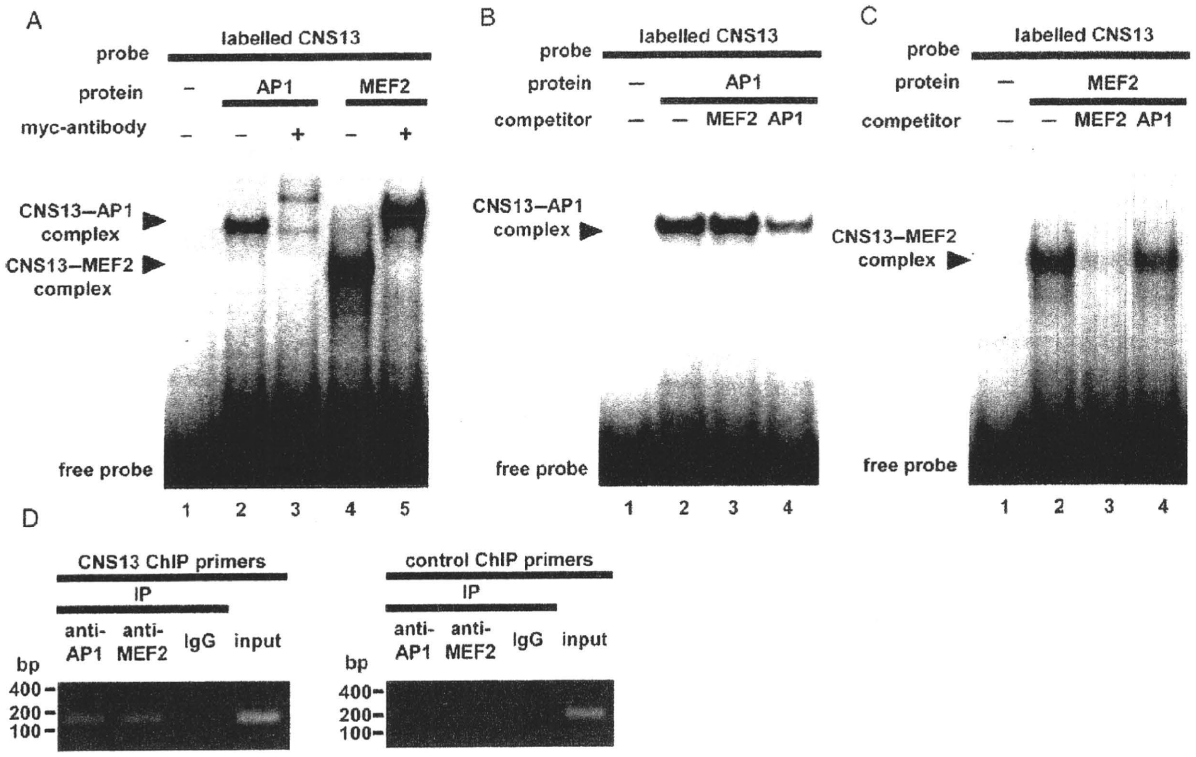

Figure 3 Electrophoretic mobility shift assay (EMSA) and chromatin immunoprecipitation (ChIP) assay using a radiolabelled CNS13 probe. (*A*) EMSA with myc-tagged AP1 and MEF2 proteins. The myc-antibody was used for the supershift assay. (*B*) Competitive EMSAs for the CNS13–AP1 complex. (*C*) CNS13–MEF2 complexes. (*D*) ChIP products using specific antibodies directed against AP1 and MEF2, or a pre-immune IgG were analysed by PCR. Input lane represents PCR products amplified from sonicated chromatin prior to immunoprecipitation. The 152 bp (left) and 200 bp (right) products correspond to CNS13 and distinct genomic regions, respectively.

the TRANSFAC database and detected MEF2- and AP1-binding motifs. As shown in *Figure 2B*, the putative MEF2- and AP1-binding sequences are perfectly conserved among several mammalian species and closely resemble their consensus sequences. These motifs, however, were not conserved in non-mammalian species. We prepared CNS13 reporter constructs harbouring mutations within the MEF2 and AP1 sites (*Figure 2C*) and examined whether enhancer activity was mediated by these sites. As shown in *Figure 2D*, a single mutation in either MEF2- or AP1-binding sequences significantly reduced transcriptional activity, whereas double mutations completely abolished CNS13-induced enhancement. These findings indicate that the *cis*-enhancer function of the CNS13 fragment is dependent on these binding sequences.

We then examined binding of MEF2 and AP1 protein to CNS13. As demonstrated by the electrophoretic mobility shift assay (EMSA) outlined in *Figure 3A*, a slow-migrating band was visualized as a result of interaction between the CNS13 probe and the myc-tagged AP1 protein (lane 2). Another complex was also formed when myc-tagged MEF2 protein was co-incubated with the CNS13 probe (lane 4). Myc-antibody also formed additional complexes (lanes 3 and 5). To precisely identify the DNA sequences recognized by MEF2 and AP1 proteins, we performed competitive EMSA using unlabelled competitors composed of partial CNS13 sequences. As shown in *Figrue 3B*, the signal for the CNS13–AP1 complex was attenuated by the addition of AP1 competitor (lane 4), but not MEF2 competitor (lane 3), indicating that the complex formation is AP1-sequence specific. In CNS13–MEF2 complex competition assays, the opposite patterns were observed (*Figure 3C*). In addition, we amplified a genomic DNA fragment of CNS13 using ChIP with antibodies directed against AP1 and MEF2 (*Figure 3D*). These findings strongly suggest that MEF2 and AP1 transcription factors bind to CNS13 and play an important physiological role in *Hcn4* transcription.

3.3 dnMEF2 resulted in reduced Hcn4 expression

Among the MEF2 family of transcription factors, *MEF2A*, *C*, and *D* are expressed in cardiomyocytes.[10] Given that AP1 is a ubiquitously expressed transcription factor, we focused our study on the physiological role of MEF2. It has previously been shown that MEF2 proteins form hetero- and homodimers and that overexpression of dnMEF2 inhibit its transcriptional activity.[11] The schematic in *Figure 4A* outlines the structure of dnMEF2. In the current study, we demonstrate that dnMEF2 significantly reduced the transcriptional activity of the luciferase reporter vectors and that the enhancer activity of CNS13 was attenuated to 12% of the control levels. When MEF2 binding motif of CNS13 was disrupted, the overexpression of dnMEF2 did not significantly inhibit the enhancer activity (*Figure 4B*).

In order to examine the physiological role of *MEF2 in vivo*, we next expressed dnMEF2 using the AAV1 vector in cardiomyocytes isolated from the inflow tract of the embryonic rat heart, a site in which the HCN4 channel is highly

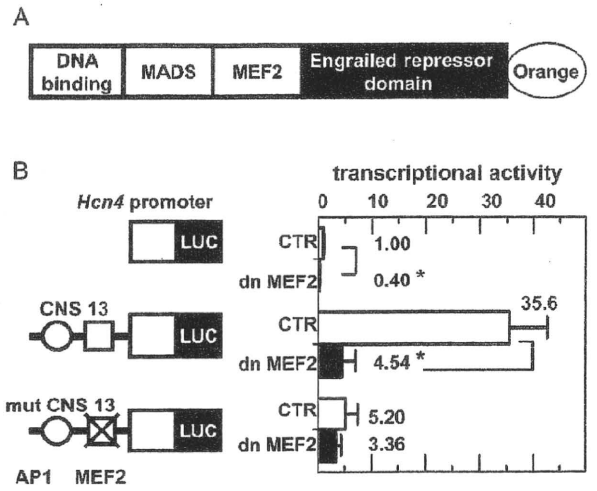

Figure 4 dnMEF2 inhibits *Hcn4* enhancer activity. (*A*) A schematic of the structure of dominant negative MEF2 mutant originated from MEF2C. (*B*) Transcriptional activity of the *Hcn4* promoter and CNS13, but not MEF2 site mutated CNS13, are significantly suppressed by dnMEF2. Along with luciferase reporter constructs, pAAV-dnMEF2 (0.3 μg) or pAAV-GFP (control; 0.3 μg) plasmids were cotransfected. Data are presented as relative values to the activity of the *Hcn4* promoter ($n = 4$; $^*P < 0.05$).

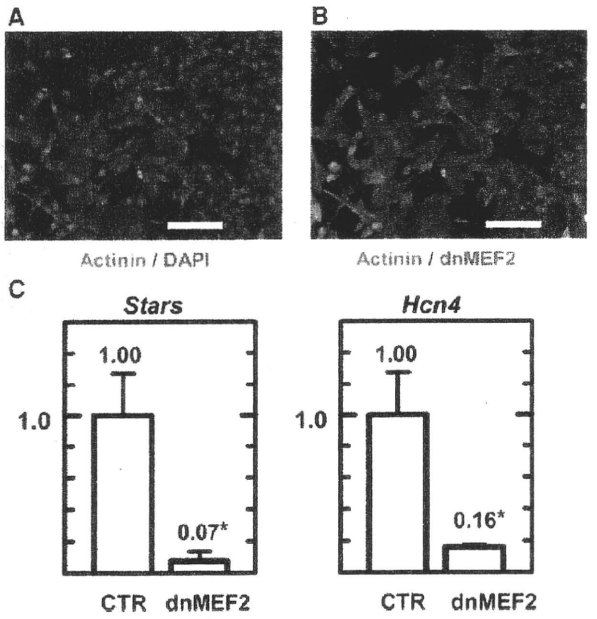

Figure 5 AAV1-dnMEF2 resulted in a reduction in *Stars* and *Hcn4* mRNA levels. (*A*). Immunofluorescent staining of cardiomyocytes for actinin (green). Nucleus is counter stained with DAPI (blue). Approximately 99% of the cells are actinin positive. Bar, 100 μm. (*B*) AAV1-dnMEF2 transfected myocytes demonstrate a nuclear orange fluorescent signal. Approximately 70% of the cells are transfected. (*C*) Relative mRNA levels measured by Q-PCR. Left, *Stars*. Right, *Hcn4*. ($n = 4$; $^*P < 0.05$ vs. control).

expressed.[12] As shown in *Figure 5A*, ~70% of cardiomyocytes was successfully transfected with dnMEF2. Three days following the transfection, *Hcn4* expression levels of Hcn4 were evaluated using real-time PCR. We also evaluated the expression levels of striated muscle activator of Rho signalling (*Stars*), which is known as a direct transcriptional target of MEF2.[13] As shown in *Figure 5A* and *B*, we found

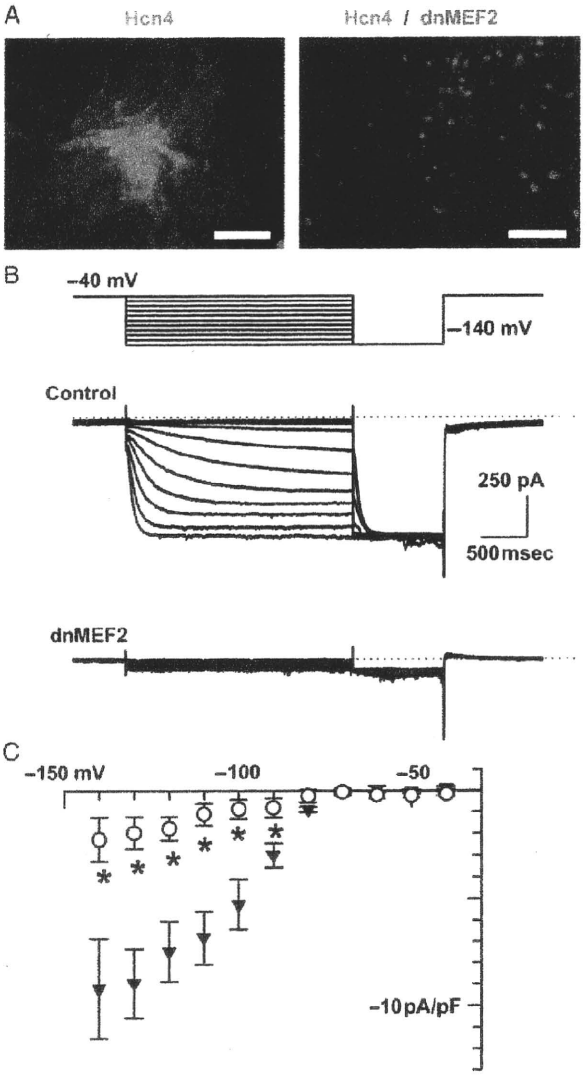

Figure 6 AAV1-dnMEF2 suppressed functional expression of the HCN4 channel. (*A*) Immunostaining for HCN4 (green). Left, control. Right, AAV1-dnMEF2. Bar, 100 μm. (*B*) I_h recorded in embryonic myocytes. The pulse protocol is shown in the top panel. The dotted line indicates the zero current level. (*C*) Current–voltage diagram of I_h. The amplitude of time-dependent current elicited by hyperpolarization was normalized by cellular capacitance. Filled triangle, control; open circle, dnMEF2 ($n = 7$; $^*P < 0.05$).

that both *Stars* and *Hcn4* mRNA levels were significantly reduced in dnMEF2-transfected myocytes, when compared with GFP-transfected myocytes as the negative control. In dnMEF2-transfected myocytes, however, the mRNA levels of HCN1 and HCN2, other types of HCN channels expressed in the heart, were not changed significantly (Supplementary material online, *Figure S1*). These channels might be regulated by different transcriptional mechanisms.[14]

We finally examined the functional expression of the HCN4 channel in embryonic myocytes transfected with dnMEF2. As shown in *Figure 6A* (left panel), HCN4 protein was clearly identified in control myocytes. However, only faint staining of HCN4 protein was observed in the myocytes transfected with dnMEF2 (nuclear-localized orange signals). In accordance with this, robust I_h current was also recorded in the control myocytes (*Figure 6B*, upper traces), whereas I_h

current was significantly reduced in dnMEF2-transfected myocytes (*Figure 6B*, lower traces). *Figure 6C* outlines the current–voltage diagram. The amplitude of I_h in dnMEF2-transfected myocytes was ~18% of the control myocytes. Similar results were also obtained for ES-derived cardiomyocytes (data not shown).[15]

4. Discussion

The transcription factors AP1 and MEF2 are known to play a variety of roles in the development of the heart. It has been reported that the ablation of *c-jun*, who along with *c-fos* forms the AP1 transcription factor, gave rise to the anomalies of right ventricular outflow tract and a reduction in *Cx43* expression.[16] Although we did not examine the direct physiological role of AP1 in the present study, it appears reasonable to expect that the expression of the *Hcn4* gene might also be reduced following the deletion of the AP1 protein. During development, *MEF2C* is known to be the predominant form of *MEF2* expressed in the embryonic heart. *MEF2A* and *MEF2D* became the major *MEF2* forms after birth.[10] Gene knockout of *MEF2C* results in an embryonic lethal phenotype.[17] MEF2D$^{-/-}$ mice are viable, demonstrating a weak response to hypertrophic stimulation.[18] *MEF2A* knockout mice generated on a 129Sv background die immediately following birth and demonstrate sinus arrhythmia and conduction block.[19] As the present study demonstrates that the expression of *Hcn4* is dependent on MEF2, it would be interesting to explore the ion channel expression in SAN of *MEF2A*$^{-/-}$ animals.

Recent studies have suggested that the *Nkx2-5* and *Pitx2c* transcription factors repress the expression of *Hcn4* in chamber myocardium, a result that is likely due to the inhibition of activators.[16] However, activators of *Hcn4* have not been identified in cardiomyocytes to date. The results of the current study suggest that MEF2 and AP1 may be candidate activators. The transcription factor *Tbx3*, in addition to *Hcn4*, is also specifically expressed in SAN. Ectopic expression of *Tbx3* in the atrium is known to induce *Hcn4* expression. However, it remains unclear whether *Hcn4* is a direct target of *Tbx3*.[5] Interestingly, we identified conserved MEF2- and AP1-like sequences within the *tbx3* gene locus. The spatiotemporal expression of *Tbx3* and *Hcn4* might be regulated via similar mechanisms.

MEF2 expression in the heart has been shown to be increased in the atrium.[20] Therefore, regional differences in *MEF2* expression might account in part for the spatial distribution of *Hcn4*. In this respect, it appears to be particularly important to investigate whether CNS13 is able to reproduce the spatiotemporal expression pattern of *Hcn4* in the heart. Although we have generated transgenic mice harbouring a *LacZ* reporter gene driven by the CNS13 and *Hcn4* promoter, we were unable to obtain consistent patterns of β-gal expression in embryos (data not shown). Thus, it is speculated that a combination of multiple CNSs may be required to reproduce the precise spatiotemporal expression pattern of *Hcn4*. Future studies will be required to address this question.

Supplementary material

Supplementary Material is available at *Cardiovascular Research* online.

Acknowledgements

We thank Dr M.A. Arnold for providing the dominant negative MEF2 cDNA.

Conflict of interest: none declared.

Funding

This work was supported in part by a Grant from the Vehicle Racing Commemorative Foundation and a Grant-in-Aid for Scientific Research from JSPS (#20300141).

References

1. Shram G, Pourrier M, Melnyk P, Nattel S. Differential distribution of cardiac ion channel expression as a basis for regional specialization in electrical function. *Circ Res* 2002;**90**:939–950.
2. Marionneau C, Couette B, Liu J, Mangoni M-E, Nargoet J, Lei M *et al.* Specific pattern of ion channel gene expression associated with pacemaker activity in the mouse heart. *J Physiol* 2005;**562**:223–234.
3. Ishii TM, Takano M, Xie L-H, Noma A, Ohmori H. Molecular characterization of the hyperpolarization-activated cation channel in rabbit heart sinoatrial node. *J Biol Chem* 1999;**274**:12835–12839.
4. Hermann S, Stieber J, Ludwig A. Pathophysiology of HCN channels. *Pflügers Arch* 2007;**454**:517–522.
5. Hoogaars W-M, Engel A, Brons J-F, Verkerk A-O, de Lange F-J, Wong L-Y *et al.* Tbx3 controls the sinoatrial node gene program and imposes pacemaker function on the atria. *Genes Dev* 2007;**21**:1098–1112.
6. Mommersteeg M-T, Hoogaars W-M, Prall O-W, de Gier-de Vries C, Wiese C, Clout D-E *et al.* Molecular pathway for the localized formation of the sinoatrial node. *Circ Res* 2007;**100**:354–362.
7. Pennacchio L-A, Ahituv N, Moses A-M, Prabhakar S, Nobrega M-A, Shoukry M *et al.* *In vivo* enhancer analysis of human conserved non-coding sequences. *Nature* 2006;**444**:499–502.
8. Visel A, Minovitsky S, Dubchak I, Pennacchio L-A. VISTA Enhancer Browser—a database of tissue-specific human enhancers. *Nucleic Acids Res* 2007;**35**:D88–D92.
9. Kuratomi S, Kuratomi A, Kuwahara K, Ishii TM, Nakao K, Saito Y *et al.* NRSF regulates the developmental and hypertrophic changes of HCN4 transcription in rat cardiac myocytes. *Biochem Biophys Res Commun* 2007;**353**:67–73.
10. Potthoff M-J, Olson E-N. MEF2: a central regulator of diverse developmental programs. *Development* 2007;**134**:4131–4140.
11. Arnold M-A, Kim Y, Czubryt M-P, Phan D, McAnlly J, Qi X *et al.* MEF2C transcription factor controls chondrocyte hypertrophy and bone development. *Dev Cell* 2007;**12**:377–389.
12. Li X-G, Okada T, Kodera M, Nara Y, Takino N, Muramatsu C *et al.* Viral-mediated temporally controlled dopamine production in a rat model of Parkinson disease. *Mol Ther* 2006;**13**:160–166.
13. Kuwahara K, Teg Pipes G-C, McAnally J, Richardson J-A, Hill J-A, Bassel-Duby R *et al.* Modulation of adverse cardiac remodeling by STARS, a mediator of MEF2 signaling and SRF activity. *J Clin Invest* 2007;**117**:1324–1334.
14. Pachucki J, Burmeister LA, Larsen PR. Thyroid hormone regulates hyperpolarization-activated cyclic nucleotide-gated channel (HCN2) mRNA in the rat heart. *Circ Res* 1999;**85**:498–503.
15. Yanagi K, Takano M, Narazaki G, Uosaki H, Hoshino T, Ishii T *et al.* HCN and Cav3 channels confer automaticity of embryonic stem-derived cardiomyocytes. *Stem Cells* 2007;**25**:2712–2719.
16. Jochum W, Passegue E, Wagner EF. AP-1 in mouse development and tumorigenesis. *Oncogene* 2001;**20**:2401–2412.
17. Lin Q, Schwarz J, Bucana C, Olson E-N. Control of mouse cardiac morphogenesis and myogenesis by transcription factor MEF2C. *Science* 1997;**276**:1404–1407.
18. Kim Y, Phan D, vanRooij E, Wang D-Z, McAnally J, Qi X *et al.* The MEF2D transcription factor mediates stress-dependent cardiac remodeling in mice. *J Clin Invest* 2008;**118**:124–132.
19. Naya F-J, Black B-L, Wu H, Bassel-Duby R, Richardson J-A, Hill J-A *et al.* Mitochondrial deficiency and cardiac sudden death in mice lacking MEF2A transcription factor. *Nat Med* 2002;**11**:1303–1309.
20. Zhao X-S, Gallardo T-D, Lin L, Schageman J-J, Shohet R-V. Transcriptional mapping and genomic analysis of the cardiac atria and ventricles. *Physiol Genomics* 2002;**12**:53–60.

循環器科，66(4)：472-480，2009

Lecture

解　説

iPS細胞研究の現状と展望*

山　下　　潤**

Key Words : embryonic stem cells, induced pluripotent stem cells, regeneration, differentiation

はじめに：iPS細胞登場の背景と意義

ES細胞(胚性幹細胞；embryonic stem cells)はマウスやヒトの早期胚(胚盤胞；blastocyst)の段階において，将来胎仔を形成する内細胞塊(inner cell mass)と呼ばれる部位を取り出して樹立した細胞株であり，体中すべての種類の細胞に分化することのできるいわゆる万能の幹細胞と考えられている．マウスES細胞の樹立は1981年であり，マウスES細胞から拍動心筋細胞が誘導されることが1985年には報告されているが，ES細胞の医学・生物学における大きな貢献は，再生医学ではなくノックアウトマウスなどのさまざまな遺伝子改変マウスの樹立を可能にしたことであった．実際，マウスES細胞を樹立したマーティン・エバンス博士は，2007年のノーベル医学生理学賞をノックアウトマウスの開発を行った研究者らと共同受賞している．1990年代後半から，神経幹細胞の発見など成体の中に存在する体性幹細胞/組織幹細胞に関する研究とともに，ES細胞を含めた幹細胞の再生医学応用に関する研究が急速に盛んになってきた．1998年末のヒトES細胞樹立により，幹細胞の再生医療応用はさらに現実味を帯びて語られるようになってきた．しかし，ヒトES細胞においては，①技術・安全面の問題，特に未分化ES細胞があやまって移植されると奇形腫を形成する可能性がある，ということに加えて，②倫理面の問題，すなわち，i)ヒトES細胞の樹立の際にヒト受精卵を壊す必要がある，ii)免疫による拒絶を受けないES細胞を樹立するためにヒト体細胞クローン胚(成体細胞の核を除核した未受精卵に核移植したクローン胚)を作る必要が考えられる，ということが実際の応用への大きな障壁になっていた．こうした状況を背景に生まれてきた新しい幹細胞がiPS細胞(人工多能性幹細胞；induced pluripotent stem cells)である．

iPS細胞は線維芽細胞など分化した細胞に特定の遺伝子群(Oct3/4, Sox2, Klf4, c-mycなど)を導入することにより，ES細胞様の万能の幹細胞の性質を持たせることに成功した細胞であり，形態，遺伝子発現パターンに加えて，*in vitro*での分化能力や，iPS細胞をもとに最終的にiPS細胞由来のマウス個体を作製できることなど，ES細胞としての大きな特性を満たしている．最初のiPS細胞は2006年に京都大学の山中らによって報告された[1]．2007年には山中らおよびトムソンら[2][3]，その後さらに多くのほかのグループによりヒトiPS細胞の樹立が報告された．ヒトiPS細胞はヒトES細胞において認められた倫理的問題，上記の②-i)，ii)を一気に回避できる画期的発明であり，「iPS細胞を用いてすぐにも再生医療が実現でき

* iPS cell research—hope and hype—.

** Jun K. YAMASHITA, M.D., Ph.D.: 京都大学再生医科学研究所幹細胞分化制御研究領域/京都大学物質—細胞統合システム拠点iPS細胞研究センター〔〒606-8507 京都市左京区聖護院川原町53〕; Laboratory of Stem Cell Differentiation, Stem Cell Research Center, Institute for Frontier Medical Sciences/Center for iPS cell Research and Application (CiRA), Institute for Integrated Cell-Material Sciences (iCeMS), Kyoto University, Kyoto 606-8507, JAPAN

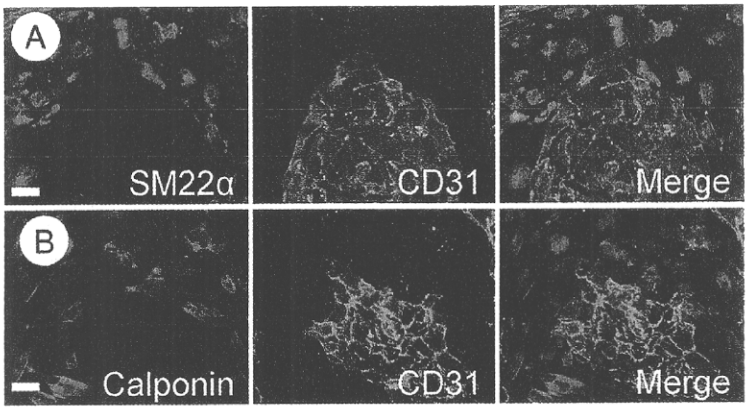

図1　マウスiPS細胞からの血管内皮・壁細胞分化
マウスiPS細胞由来Flk1陽性細胞をVEGFおよび血清存在下で培養することにより，CD31陽性内皮細胞（緑）とSM22α（A）またはカルポニン（B）陽性壁細胞（赤）が選択的に誘導される．（文献[8]より改変）

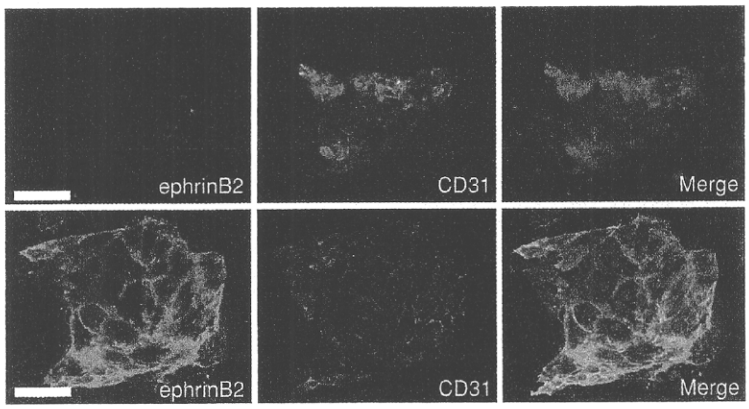

図2　マウスiPS細胞からの動静脈内皮細胞分化
Flk1陽性細胞をVEGFおよび血清存在下で培養した場合，その大部分がCD31陽性/ephrinB2陰性の静脈内皮細胞となる（上段）．VEGFに加え8bromo-cAMPを投与しcAMPシグナルを活性化すると，CD31陽性/ephrinB2陽性動脈内皮細胞が出現する（下段）．（文献[8]より改変）

るのではないか」というような，ある種の熱狂を生み出した．しかし，iPS細胞には依然として上記①の奇形腫の問題は存在しているし，iPS細胞特有の「遺伝子導入による細胞変異・がん化の問題」など，新たな問題もあり，今後地道に解決すべき課題は多い．これらiPS細胞を巡る可能性と問題点について，循環器領域との関連を中心に述べることとする．

マウスiPS細胞の心血管細胞分化

筆者らはこれまで，マウスおよびヒトES細胞を用いて心血管細胞の分化再生研究を行ってきた．すなわち，マウス未分化ES細胞から，VEGF（血管内皮増殖因子；vascular endothelial growth factor）の受容体の一つであり，血管内皮・血球の前駆細胞や中胚葉細胞のマーカーでもあるFlk1（2型VEGF受容体；VEGF receptor-2）を発現する細胞を誘導し，Flk1陽性細胞を共通の前駆細胞として，血管内皮細胞，血管壁細胞，血球細胞，心筋細胞といった循環器系細胞を系統的に分化誘導することに成功している[4)5)]．この新しい分化誘導システムを用いて，ES細胞由来の心筋前駆細胞の同定[5)]や動静脈リンパ管内皮細胞をそれぞれES細胞から誘導すること[6)7)]にも成功し

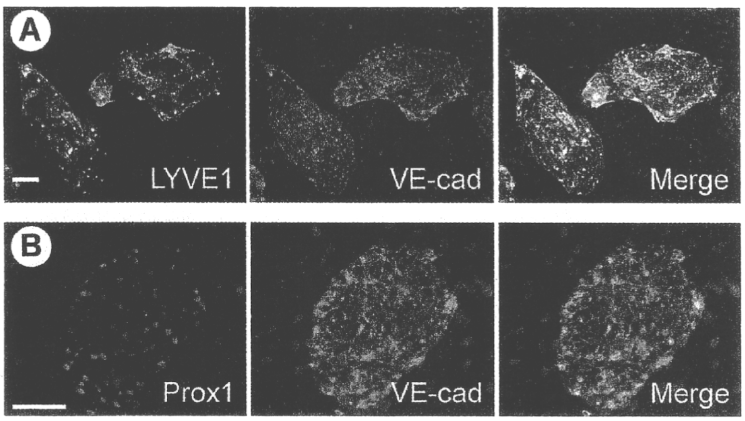

図3　マウスiPS細胞からのリンパ管内皮細胞分化
Flk1陽性細胞をOP9ストローマ細胞上で培養することにより，LYVE1陽性(A)またはProx1陽性(B)かつVE-カドヘリン陽性のリンパ管が誘導される．
（文献[8]より改変）

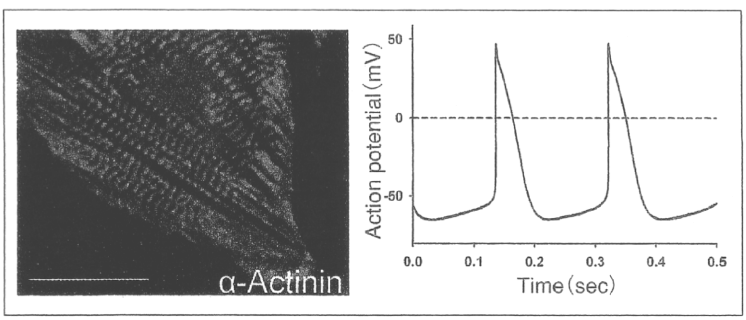

図4　マウスiPS細胞からの心筋細胞分化
Flk1陽性細胞をOP9ストローマ細胞上で培養することにより拍動心筋細胞が出現する．拍動細胞はsarcomere構造を示し(左：赤；アクチニン染色)，ペースメーカー細胞様の活動電位を示す(右)．
（文献[8]より改変）

ている．ヒトES細胞からの血管細胞の誘導や虚血モデルへの移植実験などにも関与している(京都大学内分泌代謝内科との共同研究)．このマウスES細胞の系統的心血管細胞分化システムをマウスiPS細胞に導入し，筆者らはいち早くiPS細胞からのこれら心血管細胞の分化誘導に成功した[8]．すなわち，未分化マウスiPS細胞をLIF(leukemia inhibitory factor)非存在下に培養することによりFlk1陽性細胞が誘導された．Flk1陽性細胞をVEGFおよび血清存在下に培養することにより，主に静脈を中心とする内皮細胞および壁細胞が(図1)，VEGFに加えてcAMPシグナルを刺激することにより動脈内皮細胞が(図2)，OP9ストローマ細胞上で培養することにより血球，リンパ管内皮細胞(図3)，心筋細胞が(図4)，それぞれ誘導された．マウスiPS細胞からのFlk1陽性細胞，(動静脈リンパ管)内皮細胞，壁細胞の分化様式，分化効率などはほとんどマウスES細胞と変わりがなかった．このように，マウスES細胞とマウスiPS細胞はほぼ完全に同等な心血管分化能と分化動態を示し，マウスES細胞と同様に系統的に心血管細胞を分化誘導することが可能であった(図5)．また，iPS細胞由来細胞の担がんヌードマウスへの細胞移植実験により，iPS細胞由来血管細胞が内皮および壁細胞として生体内血管新生に寄与しうることも確認している(図6)(未発表)．ただし，マウスiPS細胞を樹立する際に外来性に導入された遺伝子群の発現が長期分化培養中に再上昇したようにみえる例が観察された．明らかにがん化したような細胞や未分化になった細胞

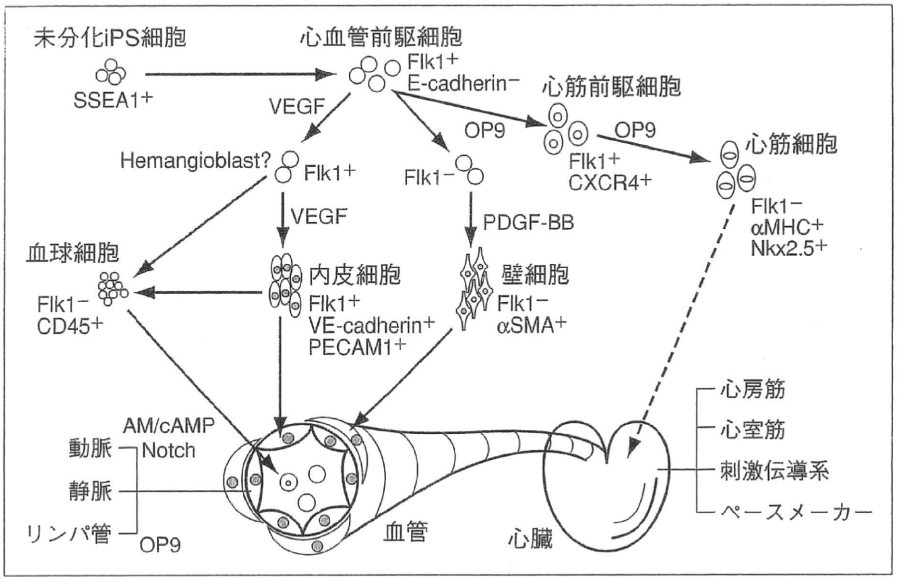

図5　マウスiPS細胞からの系統的心血管細胞分化
マウスiPS細胞から誘導したFlk1陽性細胞を共通の前駆細胞として，心血管系の構成細胞である血管内皮，壁細胞，心筋細胞，さらには動静脈リンパ管内皮細胞や種々の心筋細胞を系統的に分化誘導することができる．（文献[10]より改変）

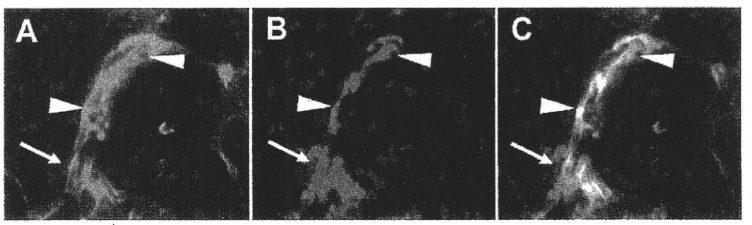

図6　マウスiPS細胞由来血管細胞による生体内血管新生
ヌードマウスの腫瘍周囲に移植されたマウスiPS細胞由来血管細胞は成体内再生に寄与する．A：CD31陽性内皮細胞(緑)．B：iPS細胞由来細胞(赤)．C：合成画像．核(青)．iPS細胞由来CD31陽性内皮細胞(矢頭)およびそれに隣接してiPS細胞由来CD31陰性壁細胞(矢印)が認められる．

が出現することはなかったが，ES細胞とは異なりiPS細胞独特の問題である導入遺伝子の影響については慎重に対応する必要があると考えられた．ほかにマウスiPS細胞からの心血管細胞分化に関しては，心筋細胞を誘導したとの報告[9]および筆者らに類似した分化システムを用いた心血管細胞分化の報告[10]と血管平滑筋分化の報告[11]などがある．

ヒトiPS細胞の心血管細胞分化

筆者らはヒトiPS細胞の心血管細胞分化にも取り組んでいる．ヒトES細胞の維持培養条件に準じた環境で誘導・樹立されたヒトiPS細胞は，その維持および分化誘導においてもヒトES細胞に類似した動態を示した．筆者らは，ヒトES細胞において報告されている心筋分化誘導法[12]に準じて培養することにより，自己拍動する心筋細胞コロニーの誘導にすでに成功している．心筋に特徴的なsarcomereの形成や自己拍動に同調したCa^{2+}の取り込みなど，形態的機能的特性も確認している(未発表)．また，胚様体(embryoid body)法を用いてヒトiPS細胞から心筋を誘導した報告が2009年2月に最初になされ[13]，その後日本からも胚様体法を用いて薬剤に反応する心筋細胞

を誘導したことが報告されている[14)15)]．血管に関しては，京都大学のグループがヒトES細胞と同様の2段階分化誘導法を用いて，ヒトiPS細胞から血管内皮細胞および壁細胞を誘導することに成功している[16)]．

マウスES細胞とマウスiPS細胞，ヒトES細胞とヒトiPS細胞はそれぞれ維持培養法，分化誘導法などにおいてほとんど同等の特性を有していると考えられる．今後のiPS細胞研究においては，マウスおよびヒトES細胞研究がその土台となり，また常に比較対象のスタンダードとなると考えられる．iPS細胞の出現によって，ES細胞研究は衰退するどころかさらにその重要性を増していると考えられる．

iPS細胞研究の臨床への貢献

ES細胞，iPS細胞研究の循環器領域における意義はやはり心血管再生治療への応用が中心的に期待されると考えられるが，それ以外にも患者特異的モデル細胞の構築という新しいアプローチができることにより，病態解明や創薬治療応用など，さまざまな形での臨床面への貢献が可能である．

1．誘導細胞の細胞移植応用

ヒトiPS細胞は，ヒトES細胞に存在した倫理面の問題，および患者特異的iPS細胞を樹立できることにより移植免疫の問題も回避できるため，細胞移植による再生医療応用が期待されている．循環器領域においても，心筋再生による心筋梗塞や心筋症その他の心不全治療，血管再生による虚血性疾患の治療，生物学的ペースメーカーによる洞不全症候群の治療などが細胞治療ターゲットとして想定される．しかし，ヒトiPS細胞を用いたこれら細胞治療の実現に至るまでには数多くの乗り越えるべきハードルが残っている．

(1)効率的心血管分化誘導法および純化法の開発

ヒトの心筋梗塞においては10^9個オーダーに至る心筋細胞が死ぬともいわれている．そのレベルの細胞数を用意することが可能な効率的誘導法を開発する必要がある．現在までで最も効率がよいと考えられるヒトES細胞からの心筋分化誘導法において，ヒトES細胞1個から心筋細胞3個と報告されている[17)]．また，ヒトiPS細胞はヒトES細胞と同様に奇形腫を形成するので，未分化ヒトiPS細胞を厳密に除去できる細胞純化法が必要である．

(2)移植用細胞の開発

最終的にヒトに対して細胞を移植するためには，単に細胞を誘導して純化するということだけでは不十分で，GMP基準の医薬品と同様な品質管理のもとに移植用細胞を用意できるようにする必要がある．もとになるiPS細胞から血清やフィーダー細胞なしで一貫して培養して，分化誘導・純化が行えるようにする必要があり，(1)から(2)の間には実は大きな隔たりがある．

(3)細胞移植法の開発

(1)，(2)を経て用意された細胞をヒトに移植する際に，いかなる細胞群をどのような方法をもって移植すれば，有効かつ安全であるかを評価していく必要がある．前臨床段階ではサルなどの大型動物を含めたスタディで評価する必要がある．最近，iPS細胞を未分化のままで20万個をマウス心筋梗塞モデルに移植すると，奇形腫の出現は認めずに心筋，血管に分化して心機能が回復したという報告がなされている[18)]．一方，マウスiPS細胞由来神経細胞移植の実験では，0.05%以下の未分化細胞の混入(100個以下/合計)でも奇形腫を形成したとの報告もある[19)]．モデルや臓器の違いがあるとはいえ，こうした大きな落差を持った報告がなされることは，細胞移植法の評価の大きな問題点である．

(4)ヒトにおける評価

(1)～(3)を経てようやくヒトへの応用が可能となると考えられる．実験的医療としての患者への細胞移植例や有効例などは比較的早く数年単位で報告されるかもしれない．しかし，1つの細胞治療法が安全性と有効性の確認を経て一般的に使用される治療法として確立されるまでには，通常の薬剤と同等以上の多大な労力と時間を要する可能性がある．

2．患者特異的モデル細胞

患者自身から細胞を採取し患者特異的なiPS細胞を樹立できるというiPS細胞にしかない特性は，移植免疫を回避した細胞治療ということだけでなく，まったく新しい形で病態の解明や創薬への応用が可能である[20)21)]．

(1)病態解明

心筋症，QT延長症候群，洞不全症候群など，心臓を構成する細胞そのものに起因すると考えられる疾患が中心となると思われるが，患者自身の細胞からiPS細胞を樹立し，そこから該当する細胞を分化誘導し種々のモデル細胞を構築できることは，病態解明にまったく新しい手段を提供する．すなわち，これまではごく少量の生検サンプルの解析に限局されていたものが，個々の症例から生きた細胞を潤沢に得られることにより，標的細胞の遺伝子解析，機能解析や薬剤の効果判定などを，実際の症例に関して繰り返し行うことが可能となる．原因遺伝子不明の症例においてもモデル細胞が構築できるので，モデル細胞を用いた原因遺伝子探索も可能となる．このように，病態解明に向けたアプローチの方法は飛躍的に増大すると考えられる．

(2)創薬応用

iPS細胞の創薬応用には大きく，新規薬剤の探索と薬剤安全性試験への応用の2つが考えられる．疾患モデル細胞を用いて，同細胞の異常を改善する新規薬剤や疾患特異的に作用する薬剤などの探索が可能となる．また，培養下における分化モデルを用いることにより，心筋分化促進物質などの新たな生理活性物質の探索も可能となる．筆者らは，マウスiPS細胞を用いて3次元培養下における血管構造形成モデルを構築し，新規海洋生物由来HDAC(ヒストン脱アセチル化酵素)阻害物質azumamideの血管形成抑制作用を示すことに成功した[22]．同モデルを用いた血管形成抑制または促進物質の探索が可能と考えられる．さらに，こうしたシステムを患者特異的iPS細胞を用いて構築することにより，疾患特異的作用物質の探索などにも展開可能と考えられる．

受精卵を用意することが必要であるヒトES細胞と比べて，iPS細胞は数多くの細胞株を樹立しやすくiPS細胞バンクが構築しやすい．そこから細胞を誘導してarray(アレイ)化することにより，種々のヒトモデル細胞パネルのようなものを構築することができる．こうしたヒトモデル細胞パネルは薬剤の安全性試験に応用可能と考えられる．たとえば，千人分や一万人分などの心筋細胞や肝細胞を並べたパネルを用いて薬剤の細胞毒性をスクリーニングすることにより，稀に発生する心毒性や肝障害などを事前に検出できるかもしれない．さらには，障害を起こす細胞を解析し原因を明らかにすることにより，副作用を起こす症例を事前に特定し投薬を避ける「テーラーメード医療」に貢献しうる可能性もある．

3．その他動物モデルへの応用

循環器病関係のモデル動物には，マウスモデルばかりでなくマウス以外の動物種のものが数多くある(高血圧自然発症ラット，糖尿病モデルラット，心筋症ハムスターなど)．これらモデル動物からのiPS細胞の樹立が可能となれば，モデル動物と同動物由来細胞を用いて，動物モデルと細胞実験を相互対応させながら新しい病態の解析を行うことなどが可能となると考えられる．

iPS細胞研究の今後

iPS細胞に関する研究は今後，iPS化(初期化)機構に関するもの，iPS細胞そのものを利用したもの，iPS化という現象を利用したものなど，多岐にわたって進められると思われる．

1．iPS細胞の改良

iPS細胞は当初，3～4個の遺伝子をレトロウイルスを用いて導入することにより誘導されているが，細胞治療に用いることができるレベルのiPS細胞を樹立するためには誘導法，誘導効率などの改良が必要である．

(1)c-mycトランスジーンなしiPS細胞

iPS細胞誘導に用いた4因子の1つであるc-mycはがん遺伝子の一つであり，実際，mycありiPS細胞由来のマウス個体では効率にがんが発生した．その後，mycを除いた3因子でもiPS細胞誘導が可能となったが，mycなしiPS細胞由来マウス個体ではがんの発生がほとんど認められなくなった[23]．

(2)レトロウイルスなしiPS細胞

現在，iPS細胞誘導にはレトロウイルスによる遺伝子導入が行われている．レトロウイルスにより導入された遺伝子はゲノム上のどこかに組み込まれることになるので，導入遺伝子が組み込まれた場所によってはがん化を含む種々の細胞の変異をもたらす可能性がある．レトロウイルスを用いずゲノムをintactに保ったままの遺伝